

Anomalous diffusion of active Brownian particles in responsive elastic gels: Nonergodicity, non-Gaussianity, and distributions of trapping times

Koushik Goswami ^{*}

*Institute of Physics and Astronomy, University of Potsdam, 14476 Potsdam, Germany
and Physics Division, National Center for Theoretical Sciences, National Taiwan University, Taipei 106319, Taiwan*

Andrey G. Cherstvy [†]

Institute of Physics and Astronomy, University of Potsdam, 14476 Potsdam, Germany

Aljaz Godec [‡]

Mathematical bioPhysics Group, Max Planck Institute for Multidisciplinary Sciences, 37077 Göttingen, Germany

Ralf Metzler [§]

*Institute of Physics and Astronomy, University of Potsdam, 14476 Potsdam, Germany
and Asia Pacific Center for Theoretical Physics, Pohang 37673, Republic of Korea*



(Received 28 July 2024; accepted 24 September 2024; published 29 October 2024)

Understanding actual transport mechanisms of self-propelled particles (SPPs) in complex elastic gels—such as in the cell cytoplasm, in *in vitro* networks of chromatin or of F-actin fibers, or in mucus gels—has far-reaching consequences. Implications beyond biology/biophysics are in engineering and medicine, with a particular focus on microrheology and on targeted drug delivery. Here, we examine via extensive computer simulations the dynamics of SPPs in deformable gellike structures responsive to thermal fluctuations. We treat tracer particles comparable to and larger than the mesh size of the gel. We observe distinct trapping events of active tracers at relatively short times, leading to subdiffusion; it is followed by an escape from meshwork-induced traps due to the flexibility of the network, resulting in superdiffusion. We thus find crossovers between different transport regimes. We also find pronounced nonergodicity in the dynamics of SPPs and non-Gaussianity at intermediate times. The distributions of trapping times of the tracers escaping from “cages” in our quasiperiodic gel often reveal the existence of two distinct timescales in the dynamics. At high activity of the tracers these timescales become comparable. Furthermore, we find that the mean waiting time exhibits a power-law dependence on the activity of SPPs (in terms of their Péclet number). Our results additionally showcase both exponential and nonexponential trapping events at high activities. Extensions of this setup are possible, with the factors such as anisotropy of the particles, different topologies of the gel network, and various interactions between the particles (also of a nonlocal nature) to be considered.

DOI: [10.1103/PhysRevE.110.044609](https://doi.org/10.1103/PhysRevE.110.044609)

I. INTRODUCTION

A. Active particles: Phenomena and models

Natural and man-made active particles [1–15] typically perform out-of-equilibrium [16], externally driven motion. They are ubiquitously used as a paradigmatic model of active and living matter [17]. The broad palette of theoretical models [1,2,4]—ranging from all-atom computer simulations to continuous descriptions—utilized to describe active-matter behaviors, have to account for the absence of detailed balance, for irreversibility of active processes in time, and for (often present) multibody long-ranged interactions of particles

(e.g., of hydrodynamic nature [12,18,19] such as in aqueous “wet”-active-matter environments). These models target often specific physical mechanisms and principles of active or facilitated transport. Its features are decisively different from those of thermally driven passive Brownian motion (BM) [20], a process with a Gaussian probability-density function (PDF) of displacements [21,22].

In recent years, this area of active-particles research led to a flurry of approaches to investigation of active matter, with a multitude of applications at different length- and time-scales. Active tracers can be realized as, e.g., swimming [23] and swarming [24] bacteria [25–33], persistently moving motor proteins [34–38], both pro- and eukaryotic motile cells of various types [7,39,40]. For their self-locomotion, some active particles harness energy from internal chemical reactions, such as of ATP hydrolysis. Further examples of actively propelled “particles” include some algae [18,41,42], amoebae [7,43,44], slime molds [45], protozoa [46],

^{*}Contact author: goswamikoushik10@gmail.com

[†]Contact author: a.cherstvy@gmail.com

[‡]Contact author: agodec@mpinat.mpg.de

[§]Contact author: rmetzler@uni-potsdam.de

run-and-tumble bacteria [47,48], hydra [49], some flagellated locomotive eukaryotic cells [50], fish-keratocyte cells [51], and spermatozoa [52,53]. On much larger scales, the motion of birds [54], of schools of fish [55], and of land-bound animals [56–58] also relies on active motion. Artificial active systems—such as chemically, acoustically, or magnetically powered micro-robots and micro-swimmers [6,59–61]—have also been recently developed for potential applications in medicine, security, and environmental sustainability [62,63]. Inside biological cells, active motor-driven motion is largely responsible for distant and controlled transport of larger cargos, while smaller entities can be effectively transported by—often uncontrolled and nondirectional—passive-diffusion-based motion.

From a modeling perspective, the migration of self-propelled particles (SPPs) through porous media has been explored in a number of previous studies [64–67], revealing, e.g., intermittent trapping and escape events via hopping from pores or cavities present in a network. In Refs. [68–71] the dynamical behavior of SPPs in viscoelastic [72] and in complex fluids was examined, with a conclusion of finding *enhanced* translational and/or rotational [33,73–75] dynamics. The effects of crowding [76–78] on the dynamics of membrane constituents [79,80] and onto the looping kinetics of polymer chains were also reported [81,82]. The translational and rotational diffusion of SPPs—as well as of nonspherical passively diffusing particles [74]—in densely packed glass-forming colloidal suspensions [83–85] was the subject of several studies as well. These investigations of SPPs predominantly revealed an enhanced motion of active tracers at packing fractions below those of the glass transition, while a dynamically arrested state of the probe was noted at densities above those of the glass transition.

The diffusion of particles is generally called anomalous when it is described by the ensemble-averaged mean-squared displacement (MSD) of a power-law form [21,22,76,86–91]

$$\langle x^2(t) \rangle \propto t^\nu, \quad (1)$$

where $\nu \neq 1$, as compared to BM with $\nu = 1$ [20]. This law has been firmly established over the past two decades, largely attributed to advances in single-particle-tracking techniques [92,93]. Examples of such systems encompass macromolecular diffusion in cyto- and nucleo-plasmatic environments, the transport of vesicular cargos inside living cells, protein translocation through nuclear nanopores, the dynamics of proteins on the cell membranes, to mention a few cell-related examples; see Refs. [22,94].

The diffusion of SPPs in dilute and semidilute polymer-based solutions was studied in Refs. [95–97], capturing a variety of anomalous dynamical behaviors (1). Particularly, the motion was found to exhibit non-Gaussian characteristics, with an enhanced diffusivity at higher activity of SPPs. In some cases, intermediate *subdiffusion* was attributed to a stickiness of the SPPs to medium's components, to high densities of crowding agents, and to certain caging effects induced by surrounding polymer chains. In contrast, transient *superdiffusion* was naturally found to dominant at higher activities of the diffusing SPPs [95,97].

Although known already since the work of Fürth [1] for longer than a century, during the last decade or so the study

of SPPs exhibits a renaissance. We mention here only some recent representative studies from experimental [11,13,83,98–101], theoretical [3–6,14,102–120], and computer-simulation [17,33,66,82,121–133] communities. Active particles are driven out of equilibrium due to a continuous energy intake, yielding the statistics of motion (often) violating the principles of detailed balance [134,135]. The dynamics of active particles in the presence of external potentials [102,136–139] and with mutual interactions [4,140–143] can potentially give rise to self-organization [12]. Chiral [144,145] active particles [146,147], chiral active disks [115], active particles in shear flows [148], and the effects of active motion on the precision of signaling [149,150] were also considered recently. The transition from active motion to anomalous diffusion for *Bacillus subtilis* confined in hydrogel matrices was recently studied [151].

Unlike passive motion, active tracers can move persistently in a specific direction over a certain timescale, the so-called persistence time. While free diffusion of SPPs is well understood within a framework of multiple theoretical models [4], investigations on actively driven motion in real-world environments—often characterized by a number of complicating features (such as porosity, crowding, heterogeneity [152], various interactions, and some disorder) as well as responsiveness of the medium—are still ongoing [5].

B. Anomalous diffusion and elastic gel networks

In heterogeneous or/and crowded environments [76,153]—such as those inside the cell cytoplasm, in the extracellular matrix, in solutions of polyelectrolytes [154], or in a biofilm—the tracer dynamics often exhibits (at least transiently) some anomalous-diffusion features. One of the primary reasons for this is a complicated and heterogeneous architecture of diffusion media being formed, e.g., by a cross-linked, flexible, and responsive polymeric network [155,156] or a gellike formation [157]. Some long-range correlations [54] can also contribute. This hinders motions of larger tracers passing through such a meshwork, both via formation of restricted cavities, topological constraints, and also via specific particle-network interactions.

The study of diffusion of tracers in gels has gained significance in the past decade, owing to its potential applications in various fields, including rheology [157], medicine [158,159], and materials engineering [160,161]. For instance, by tracking the trajectories of tracers embedded in a gel, one can obtain valuable information about the microstructure of the network and its viscoelastic properties [162–164]. As a concrete example, tracking and examining trajectories of the tracers in hydrogels composed of mucin proteins (mucus [165]) recently enabled the researchers to categorize the degree of non-Gaussianity and of nonergodicity of diffusion, as a function of varying pH levels of the medium [157,164,166,167]. Moreover, the presence of tracers inside the meshwork can modify its rheological and electromagnetic properties; this can be used, e.g., to design novel hybrid materials [168]. With a specific knowledge of the mesh dimension to the tracer size, of mutual tracer-network affinities, and of elastic properties of the gel one can employ effective and fairly selective separation of macromolecules. The latter can, e.g., be used for

the development of clinical diagnostic tools for targeted drug delivery [159].

A number of theoretical, simulations-based, and experimental studies have been devoted to investigations of thermal motion of *passive* tracers in various polymeric networks [157,169–176]. They have often confirmed a transient subdiffusive behavior, with $0 < \nu < 1$, particularly for particles of sizes comparable to or larger than the mesh size of the gel and for tracers featuring a higher affinity to the monomers of polymer chains [170,173]. The propulsion of active particles in responsive polymeric networks is much less studied [128]. It is thus very relevant to consider the dynamics of *active* tracers of variable sizes and activities in polymer-based gel networks. This is the main subject of our current study.

Most recently, the dynamics of SPPs in a polymer network has been investigated by computer simulations for networks of a well defined, regular structure—such as that of a cubic or a diamond lattice—with each lattice point being occupied by a single gel bead [177–179]. The nearest gel beads were modeled [177–179] to be connected by springs, by double springs, or by short polymer chains. These studies have captured the interplay between activity and confinement effects onto the dynamics of mesh-sized SPPs in such a network (modeled within several theoretical models). Particularly, the self-correlation function for the mesh-sized active Ornstein-Uhlenbeck particles (AOUPs) was found [177] to be oscillatory at intermediate times, which eventually was shown to turn smoother and to become Gaussian in the long-time limit. Depending on the activity of the particles, their spreading dynamics was shown to have distinct dynamical patterns at different timescales. Below a certain activity, it was demonstrated [177] that confinement-induced subdiffusion was followed by a normal-diffusion regime. Above a certain activity, the dynamics was found to be initially superdiffusive and later diffusive [177].

In a similar study [179], an intermediate subdiffusive regime was observed for sticky active Brownian particles, whereas the dynamics was found to be superdiffusive for nonsticky particles. The trapping and hopping mechanisms were discussed in Ref. [177], revealing an exponential distribution of durations of trapping events. Furthermore, three distinct scaling behaviors of the long-time diffusivity with varying activity of the particles were identified by simulations, reflecting likely different underlying transport mechanisms.

One of the interesting features of *passive* diffusion of tracers in elastically responsive gels studied in Ref. [170] was the fact that—due to *collective fluctuations* (“breathing” events) of the gel structure—particles measurably larger than the meshwork size were still able to “advance” in the gel via subdiffusion. Our intention here for the dynamics of SPPs is to unravel an intricate interplay of obstructions imposed by the interconnected beads of the gel, of the persistence of SPP-tracers, and of cage-opening events due the internal dynamics of the gel. These effects are expected to be most pronounced for softly connected and highly responsive gels.

C. Outline of the article

In this paper, we extend the studies of diffusion of *passive* tracers in flexible gellike networks to propagation of *actively*

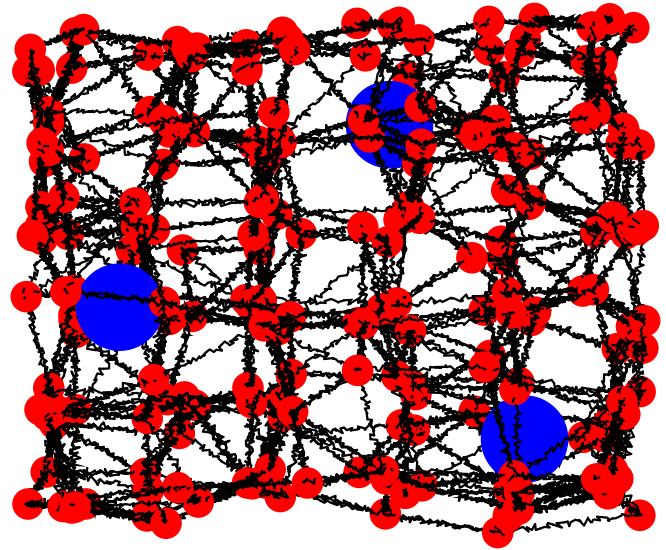


FIG. 1. Simulated 3D gel network at Péclet number $Pe = 1$, with the gel beads and tracers represented by small red and large blue spheres, respectively. The bonds between the lattice-neighboring gel beads—extending along the principal axes of the lattice and each having a fluctuating length—are shown as black springs. Video files of tracer motion for the model of AOUPs and RTPs at different Péclet numbers are provided in the Supplemental Material [180]. Note that abrupt jumps of a tracer from one side of the simulation cell to the opposite one (visible in videos) are visual artifacts of the implementation of periodic boundary conditions in all three dimensions.

driven particles in polymeric gels. The study [170] serves as a basis for our current examination. Here, we consider the motion of spherical SPPs inside a three-dimensional (3D) cross-linked flexible polymeric network; see Fig. 1. This gel network forms a cubic lattice, with all gel beads separated by one lattice spacing and connected via springs. The latter are parameterized by the Morse potential. Thus, the gel acts as a meshwork of geometrical obstacles for a diffusing tracer. The local mesh size of the gel can, however, fluctuate in response to a propagating tracer, with the degree of relative bond-length fluctuations that depends on the particle activity, the network elasticity and the tracer-to-gel affinity.

The rest of the article is organized as follows. In Sec. II the details of the model, the simulation scheme, and the dynamical variables are introduced and presented. In Sec. III we discuss the main results of the performed computer simulations, based on the extensive analysis of the behavior of a number of standard and of some new statistical quantifiers. Finally, we underline the physical consequences of the main findings. In Sec. IV we present a discussion and summarize the main conclusions.

II. MODEL

A. Dynamics of the tracers

In free 3D space, the dynamics of a single SPP in the *overdamped* limit (no inertia; see Ref. [181] for treatment of inertial effects) under the action of force F is described by the

TABLE I. List of model parameters used in simulations.

Parameter	Notation	Value	Dimension
Thermal energy	$k_B \mathcal{T}$	4.114	pN nm
Dispersion energy of the bead-tracer LJ potential	ϵ_{ig}	1.5	$k_B \mathcal{T}$
Dispersion energy of the bead-bead LJ potential	ϵ_{gg}	1.0	$k_B \mathcal{T}$
Diameter of the gel bead	σ_g	1	μm
Diameter of the tracer	σ_t	5	σ_g
Diffusion coefficient of the gel bead	D_g	1.0	$\sigma_g / \sqrt{\epsilon_{gg}}$
Thermal diffusivity of the tracer	D_t	0.2	$\sigma_g / \sqrt{\epsilon_{gg}}$
Active diffusivity of the tracer	D_{act}	Variable	$\sigma_g / \sqrt{\epsilon_{gg}}$
Péclet number	Pe	Variable	1
Equilibrium bond distance	r_{eq}	5	σ_g
Cutoff distance of the Morse potential	r_c	1.2	r_{eq}
Energy parameter of the Morse potential	ϵ_M	2.5	$k_B \mathcal{T}$
Reciprocal-width parameter of the Morse potential	h_M	$1/\sqrt{2}$	σ_g^{-1}
Activity parameter	f_{act}	Variable	$1/\sqrt{\epsilon_{gg}}$
Simulation time step	Δt	10^{-4}	$\sigma_g \sqrt{\epsilon_{gg}}$

Langevin equation

$$d\mathbf{r}(t)/dt = \mathbf{F}/\zeta_t + \boldsymbol{\eta}_{\text{th}}(t) + \boldsymbol{\eta}_{\text{act}}(t), \quad (2)$$

where $\eta_{\text{th},i}(t)$ and $\eta_{\text{act},i}(t)$ are, respectively, the thermal and active noise along the direction $\{i,j\} = \{x, y, z\}$. Here $\zeta_t = 6\pi\zeta(\sigma_t/2)$ is the drag coefficient of the tracer (ζ is the dynamical viscosity of the solvent, σ_t is the diameter of a tracer particle, and $k_B \mathcal{T}$ is the thermal energy). The indices responsible for the space directions are kept on purpose roman, not to be confused with the italicized indices for the particle number. Thermal noise features delta-type correlations in time, zero mean, and absence of correlations with respect to different axes, that mathematically can be expressed as

$$\langle \eta_{\text{th},i}(t) \cdot \eta_{\text{th},j}(t') \rangle = 2D_{\text{th}} \delta_{i,j} \delta(t - t'). \quad (3)$$

Here D_{th} is the thermal diffusivity related to the ambient temperature \mathcal{T} (denoted here slanted not to be mixed with the trajectory length T used below) via the Einstein-Smoluchowski relation,

$$D_{\text{th}} = k_B \mathcal{T} / \zeta_t. \quad (4)$$

For convenience of the reader, the main parameters of our model and of computer simulations are listed in Table I. To describe the self-propulsion of the tracer, an additional active-noise term $\boldsymbol{\eta}_{\text{act}}(t)$ with physical dimensions of velocity is introduced in Eq. (2). Such self-propulsion forces can arise, e.g., due to a metabolic activity in the form of ATP hydrolysis in cells and they drive the system out of equilibrium.

B. AOUPs versus RTPs

We consider two models of active tracers: (i) AOUPs and (ii) run-and-tumble particles (RTPs). These acronyms are related to the type of the particles, not to the underlying stochastic processes. The model of RTPs is commonly employed for modeling bacterial motion [182]. In the case of AOUPs, the magnitude of the active force is characterized by stochastic variability described by the active Ornstein-Uhlenbeck [183] process (see its description in Refs. [184–187]). In contrast, the active force remains con-

stant in the case of RTPs (see Refs. [182]) with changes in directions of particle motion following a random process. The x -component trajectories of AOUPs and RTPs are shown in Fig. 10: the fact that active forces evolve very differently in these two cases is easily noticeable. Moreover, in our study, the active force for all RTP-trajectories initially takes a *negative* value, resulting in a *negative* drift for these particles, see the inset in Fig. 10(b) and the discussion in Sec. III D. These differences between cases (i) and (ii) have implications onto the diffusive characteristics of respective active particles; see Sec. III.

A common and effective model for active noise is given by the active Ornstein-Uhlenbeck process described as [184–187]

$$d\boldsymbol{\eta}_{\text{act}}(t)/dt = -\boldsymbol{\eta}_{\text{act}}(t)/\tau_{\text{act}} + \sqrt{2f_{\text{act}}^2/\tau_{\text{act}}} \times \boldsymbol{\gamma}(t), \quad (5)$$

where $\boldsymbol{\gamma}(t)$ is a delta-correlated white Gaussian noise of a strength which scales with f_{act} . Here, the exponentially decaying correlations are

$$\langle \eta_{\text{act},i}(t_1) \eta_{\text{act},j}(t_2) \rangle = f_{\text{act}}^2 \delta_{i,j} \times e^{-|t_1 - t_2|/\tau_{\text{act}}}, \quad (6)$$

where—similarly to Eq. (3)—the Kronecker delta symbol ensures that the components of $\boldsymbol{\eta}_{\text{act}}(t)$ in different directions are mutually independent. Here, τ_{act} is the persistence time that determines the timescale over which the directionality of self-propulsion is conserved (on average) and f_{act} is the amplitude of the self-propulsion force. One can define an “active diffusivity” D_{act} in terms of f_{act} and τ_{act} as [188,189] $D_{\text{act}} = f_{\text{act}}^2 \tau_{\text{act}}$. To quantify the activity of the particles, we use the dimensionless Péclet number [6] defined via the diameter σ_t and the diffusion coefficient D_t of the tracer as

$$\text{Pe} = f_{\text{act}} \sigma_t / D_t. \quad (7)$$

Thus, the case $\text{Pe} = 0$ corresponds to a passive tracer, whereas large Pe numbers indicate high activity of the particles.

In the model of RTPs, a particle moves in a specific direction for a certain time with a constant speed v_0 and then randomly changes its direction (it “tumbles”). These running-and-tumbling modes of motion are repeated by each particle.

A change in the direction of motion is stochastic; it is often modeled by a Poisson process [190–192]. In such a model, a driven 1D particle can move only to the right or to the left; in 2D the direction of particles—expressed by the angle θ with the y axis—can generally take continuous values between 0 and 2π . This model can also be formulated discretely, such, e.g., as a four-state model with angles $\theta = \{0, \pi/2, \pi, 3\pi/2\}$ only. In 3D an additional angle ϕ with the z axis is to be parameterized; in a similar fashion, for active RTPs we adopt a model with eight possible states for 3D motion. In such a model, the RTP can thus have angles of motion $\theta = \{0, \pi/2, \pi, 3\pi/2\}$ with $\phi = \{0, \pi\}$.

Specifically, the active force in each direction can be described as a dichotomous colored noise [190,193]

$$\eta_{\text{act},i}(t) = v_0 \sigma_{D,i}(t), \quad (8)$$

where v_0 is the speed of self-propulsion and $\sigma_{D,i}$ takes the values of ± 1 following the Poissonian statistics with a fixed rate r_0 . Therefore, $\sigma_{D,i}(t) = (-1)^{n(t)}$, where $n(t) = m$ is the number of jumps during time t following a Poisson distribution

$$P(m) = (r_0 t)^m e^{-r_0 t} / m!. \quad (9)$$

The noise generated by this process features the exponential correlation function [190,191]

$$\langle \eta_{\text{act},i}(t_1) \eta_{\text{act},j}(t_2) \rangle = v_0^2 \delta_{ij} \times e^{-r_0 |t_1 - t_2|}. \quad (10)$$

Here the Péclet number can be expressed as

$$\text{Pe} = v_0 \sigma_t / D_t. \quad (11)$$

A typical trajectory of a single RTP in 2D is shown in Fig. 11. While for AOUPs the magnitude of the force can vary and the change in direction is governed by a Gaussian process, for RTPs the magnitude of the force remains constant at v_0 and the force acts only in six possible distinct directions, with changes in directions being determined by a Poissonian process.

C. Potentials and equations of motion

The gel network in its equilibrium state in the absence of active particles is represented by a cubic lattice consisting of $6 \times 6 \times 6$ gel beads, each with diameter σ_g , as shown in Fig. 1. All lattice-neighboring beads are elastically connected via the Morse potential [194]

$$U_M(r_{ij}) = \begin{cases} \varepsilon_M [e^{-2h_M(r_{ij}-r_{\text{eq}})} - 2e^{-h_M(r_{ij}-r_{\text{eq}})}] - U_c, & r_{ij} \leq r_c \\ 0, & r_{ij} > r_c \end{cases}. \quad (12)$$

Here $r_{ij} = |\mathbf{r}_i - \mathbf{r}_j|$ is the separation between the i th and the j th bead, we define $U_c \equiv U_M(r_c)$, and r_c is the cutoff distance. In Eq. (12), the parameter ε_M represents the depth of the potential, h_M determines its reciprocal width, and r_{eq} defines the equilibrium bead-to-bead distance (bond length).

To account for excluded-volume interactions, a repulsive Lennard-Jones (LJ)-type [195–197] 6-12 potential, shifted to the Weeks-Chandler-Andersen form [198,199],

$$U_{\text{LJ}}(r_{ij}) = \begin{cases} 4\epsilon_{ij} \left[\left(\frac{\sigma_{ij}}{r_{ij}} \right)^{12} - \left(\frac{\sigma_{ij}}{r_{ij}} \right)^6 \right] + \epsilon_{ij}, & r_{ij} \leq 2^{1/6} \sigma_{ij} \\ 0, & r_{ij} > 2^{1/6} \sigma_{ij} \end{cases}, \quad (13)$$

between the i th and the j th beads is used in the simulations. Here $\epsilon_{ij} = \epsilon_{\text{gg}}$ is the depth of the potential between these gel beads and $\sigma_{ij} = (\sigma_i + \sigma_j)/2$ is the effective separation between the beads. Thus, based on Eqs. (2), (12), and (13), the dynamics of the i th bead of the gel is described by the following stochastic differential equation

$$d\mathbf{r}_{i,g}(t)/dt = \zeta_g^{-1} \sum_{j,j \neq i} \mathbf{F}_{ij} + \boldsymbol{\eta}_{\text{th}}(t). \quad (14)$$

Here, ζ_g is the friction coefficient of a gel bead, $\zeta_g = 6\pi \zeta (\sigma_g/2)$, and the total force acting on each bead is

$$\mathbf{F}_{ij} = -\nabla[U_M(r_{ij}) + U_{\text{LJ}}(r_{ij})], \quad (15)$$

where $\nabla U = \sum_{k=\{x,y,z\}} \mathbf{e}_k \partial U / \partial r_k$.

The tracers diffuse inside the gel and interact with the gel beads via the repulsive LJ potentials (13) with $\epsilon_{ij} = \epsilon_{\text{tg}}$ and with

$$\sigma_{\text{tg}} = (\sigma_t + \sigma_g)/2. \quad (16)$$

Therefore, the dynamics of the i th tracer in the gel is governed by

$$d\mathbf{r}_{i,t}(t)/dt = -\zeta_t^{-1} \sum_{j=1}^{N_g} \nabla U_{\text{LJ}}(r_{ij,\text{tg}}) + \boldsymbol{\eta}_{\text{th}}(t) + \boldsymbol{\eta}_{\text{act}}(t), \quad (17)$$

where $r_{ij,\text{tg}}$ is the distance between the i th tracer and the j th bead of the gel; N_g is total number of gel beads.

Thermal agitation of the network occasionally enables cage-opening events [170] and, thereby, a passage of tracers from one cell of the gel to the next, even if the tracer size exceeds the pore size in a *static* mesh-work in the absence of thermal fluctuations (zero-temperature limit). Our toy model examines the effects of confinement and caging imposed by a polymeric interconnected or entangled gel structure on the diffusion of tracer particles. The parameters of the model were chosen on purpose so that in order to perform a motion the tracer needs to deform the network and to escape from its local “cage.” To map a structure of real-world polymeric gels to our network of the quasiperiodic gel beads, one needs to know the average mesh size of a given gel and to choose the tracer size in experiments accordingly, to induce “caging” of the tracers. Higher concentrations of intermingled polymer chains in a polymer gel result naturally in smaller average mesh sizes. The elasticity of the bead-to-bead connections is imposed in our model via the Morse potential; it characterizes the stretching characteristics and the inter-connectivity properties of polymer-polymer contacts in realistic gels.

D. Details of computer simulations

The dynamics of the tracers and of the gel beads—described by Eqs. (17) and (14), respectively—is simulated using the Euler-Maruyama method [200]. At each time step, the forces acting on the particles (both gel beads and tracers) are calculated via Eq. (15) by considering their neighbors, for each within a specified cutoff distance r_c of the Morse potential; see Table I. The computed forces are then used in the respective Langevin equations (14) and (17) in order to update the positions of each particle. For AOUPs, the active force at each time step is generated by solving Eq. (5). For RTPs, each

component of the active force takes a value of either $+v_0$ or $-v_0$, switching according to a Poissonian process with the rate r_0 ; see Eq. (8). Concretely, at each time step, a random number is generated from the uniform distribution $\mathcal{U}(0, 1)_{\text{numb}}$, and if

$$r_0 \times \Delta t > \mathcal{U}(0, 1)_{\text{numb}} \quad (18)$$

with the force currently being $-v_0$, it changes its sign in the next step to become $+v_0$. The next sign reversal occurs when the condition (18) is met again. The simulations are performed in the canonical NVT ensemble, so that the total number of particles N , the volume of the simulation box V , and the temperature of the environment \mathcal{T} are all kept constant.

We impose the periodic boundary conditions in all directions of the lattice to mimic an infinite gel network. No measurable influence of the box size on the final results of computations is expected. The periodic boundary conditions ensure that the particles leaving the simulation box on one side reenter from the opposite side. We choose an integration time step of $\Delta t = 10^{-4}$ in the simulations (see units in Table I); it is kept small to account for an increased frequency of tracer-network collisions when the tracer size is comparable to the mesh size. The initial configuration of the network is taken generally off its equilibrium state. After an extensive equilibration of the gel meshwork, $N = 15$ trajectories of the tracers with $N_{\text{steps}} = 5 \times 10^6$ steps and of length

$$T = N_{\text{steps}} \times \Delta t = 500 \quad (19)$$

are simulated and recorded. The positions of the gel beads are *not* recorded at each step of the simulations because of the enormous memory requirements (ca. 60 GB per trajectory). The simulation time of a single trajectory of this length is 60, . . . , 70 hours (hereafter, a range of a parameter is denoted this way) on a high-performance computing cluster.

E. Dynamical variables and statistical quantifiers

1. TAMSD and scaling exponent

To rationalize the dynamics of the tracers, we analyze the behavior of a number of selected relevant statistical quantities computed from the simulation data. First, for each of the recorded trajectories of length T we compute the time-averaged MSD (TAMSD) as a function of the lag time Δ , given in a continuous representation for a 3D trajectory of the i th particle $\mathbf{r}_i(t)$ by [21,22,90]

$$\overline{\delta_i^2(\Delta)} = \frac{1}{T - \Delta} \int_0^{T-\Delta} dt [\mathbf{r}_i(t + \Delta) - \mathbf{r}_i(t)]^2. \quad (20)$$

In a discrete form, the TAMSD is computed at points with the elementary step dt along the trajectory; the integral in Eq. (20) is then replaced by a sum, see the examples of such discrete analyses in Refs. [7,157,201]. To keep the expressions short, we use the notation $\overline{\delta_i^2(\Delta)}$ for the TAMSD, although it also parametrically depends on the trajectory length T . After averaging over all N available realizations, the mean TAMSD is

$$\overline{\langle \delta^2(\Delta) \rangle} = N^{-1} \sum_{j=1}^N \overline{\delta_j^2(\Delta)}. \quad (21)$$

Similarly, for a single space component in 1D one can define the respective mean TAMSD as

$$\overline{\langle \delta_x^2(\Delta) \rangle} = \frac{1}{N} \sum_{i=1}^N \frac{1}{T - \Delta} \int_0^{T-\Delta} dt [x_i(t + \Delta) - x_i(t)]^2 \quad (22)$$

and the mean fourth moment of the time-averaged displacement as

$$\overline{\langle \delta_x^4(\Delta) \rangle} = \frac{1}{N} \sum_{i=1}^N \frac{1}{T - \Delta} \int_0^{T-\Delta} dt [x_i(t + \Delta) - x_i(t)]^4. \quad (23)$$

The TAMSD-related anomalous exponent μ characterizing the variation of $\overline{\langle \delta^2(\Delta) \rangle}$ or of $\overline{\langle \delta_x^2(\Delta) \rangle}$ with the lag time Δ follows from the scaling relation

$$\overline{\langle \delta^2(\Delta) \rangle} \propto \Delta^\mu. \quad (24)$$

Thus, the lag-time-local exponent of the TAMSD $\mu(\Delta)$ is conventionally computed as the slope in log-log scale [22],

$$\mu(\Delta) = \partial \log \overline{\langle \delta^2(\Delta) \rangle} / \partial \log \Delta. \quad (25)$$

We often consider [7,22,157] the TAMSD at $\Delta/T \ll 1$ —the region featuring statistically the best sampling of the data—for extracting the short-lag-time scaling exponent $\mu(\Delta)$. Note that $\mu = 1$ corresponds to normal diffusion in the TAMSD sense, while values $\mu < 1$ or $\mu > 1$ correspond to the case of sub- or superdiffusion [21,22], respectively. For ballistic motion one gets $\mu = 2$. So, the anomaly of diffusion can realize both for the MSD (1) and for the mean TAMSD (24) [22].

2. Nonergodicity and non-Gaussianity

The MSD-to-TAMSD *nonequivalence*—in terms of the short-time scaling exponents or of the magnitudes of respective displacements—is a manifestation of the phenomenon of weak ergodicity breaking [22]. These displacement characteristics are natural to be considered for the spreading dynamics of particles in isotropic continuous-space media. The Boltzmann notion of nonergodicity [202] *per se* refers to a discrepancy of the ensemble- and time-based averages of a physical quantity.

The degree of *nonergodicity*—quantified via the degree of irreproducibility of individual TAMSD trajectories [21,22,203]—can be quantified with the so-called ergodicity-breaking parameter (here defined along the x coordinate)

$$\text{EB}_x(\Delta) = \left(\overline{\langle \delta_x^2(\Delta) \rangle} \right)^2 / \overline{\langle \delta_x^4(\Delta) \rangle} - 1. \quad (26)$$

In the field of statistics, the same parameter is known as the squared coefficient of variation (COV), in this case $\text{EB}_x(\Delta) = \text{COV}^2(\overline{\delta_x(\Delta)})$. For ergodic systems, provided particle trajectories are much longer than all characteristic times of the dynamics of a system, one expects $\text{EB}(\Delta \rightarrow 0) \rightarrow 0$. For standard BM, e.g., one gets at $\Delta \ll T$ that [204,205]

$$\text{EB}_{\text{BM}}(\Delta) = 4\Delta/(3T). \quad (27)$$

For nonergodic processes in general, the property $\text{EB}(\Delta \rightarrow 0) \rightarrow 0$ is no longer true; the functional form of $\text{EB}(\Delta) \rightarrow 0$ as $\Delta \rightarrow 0$ decay is also an intricate, process-specific property

(it is beyond the scope of this study; see Refs. [22,205–208]). In terms of a variable [209]

$$\xi_x(\Delta) = \overline{\delta_x^2(\Delta)} / \langle \overline{\delta_x^2(\Delta)} \rangle, \quad (28)$$

the EB parameter (26) becomes [22]

$$\text{EB}_x(\Delta) = \langle \xi_x^2(\Delta) \rangle - 1. \quad (29)$$

The system is considered ergodic when for all available trajectories $\xi_x(\Delta) \approx 1$ at $\Delta \ll T$, i.e., a complete reproducibility of all TAMSD trajectories in a data set [22].

To quantify deviations of the tracer dynamics from Gaussianity, below we compute a *modified* non-Gaussianity parameter (NGP), given in 1D by [76,79]

$$\gamma_x(\Delta) = \overline{\delta_x^4(\Delta)} / [3\overline{\delta_x^2(\Delta)}^2]. \quad (30)$$

Note that, to be able to present the results for the NGP in log-log scale, we *do not* subtract unity in Eq. (30), contrary to the common definition of such a parameter in the literature [76]. A perfectly Gaussian process then features $\gamma_x = 1$. For $\gamma_x(\Delta) > 1$ [or $\gamma_x(\Delta) < 1$] broader (or narrower) than Gaussian distributions are typically observed. A more comprehensive way, as compared to the non-Gaussianity parameter, is to compute the Kullback-Leibler “distance” [210] from a given to the standardized Gaussian distribution.

Note that the NGP is related to the kurtosis K of a distribution because both contain the fourth moment. The kurtosis of a given distribution minus the kurtosis of a Gaussian distribution, $EK = K - 3$, is called the excess kurtosis. For instance, $EK = 0$ for the Gaussian and $EK = 3$ for the Laplaceian distribution. A distribution with a positive and negative value of the excess kurtosis EK is referred to as lept- and platy-kurtic, respectively. Lastly, if defined in terms of the standardized central second and fourth moments of particle displacements, the definition (30) would yield the kurtosis divided by 3.

3. Distributions of displacements and of angles

Another important quantifier characterizing the dynamics is the PDF of tracer displacements $p(x, t)$ (or the self-part of the van Hove correlation function (HCF) [211]). The PDF in 1D can be computed as the probability of finding a tracer within a small region $[\chi, \chi + d\chi]$ at time $(t + \Delta)$ as measured from its position at time t (along a single trajectory). Therefore, the ensemble-time-averaged displacement-distribution function can be written as [170]

$$G_{\text{tt}}(\chi, \Delta) = \frac{C^{-1}}{N} \sum_{i=1}^N \frac{\int_0^{T-\Delta} dt \delta\{[x_{i,t}(t + \Delta) - x_{i,t}(t)] - \chi\}}{T - \Delta}, \quad (31)$$

where C^{-1} is the normalization constant. Similarly, in 3D this function can be expressed as $P_{\text{tt}}(r, \Delta) = 4\pi r^2 G_{\text{tt}}(r, \Delta)$ or

$$P_{\text{tt}}(r, \Delta) = \frac{C^{-1}}{N} \sum_{i=1}^N \frac{\int_0^{T-\Delta} dt \delta[|\mathbf{r}_{i,t}(t + \Delta) - \mathbf{r}_{i,t}(t)| - r]}{T - \Delta}, \quad (32)$$

where the factor $4\pi r^2 dr$ is the spherical volume element with radius in a range $[r, r + dr]$. To address the question of how the gel dynamics collectively affects the tracer diffusion,

we compute the cross-HCF for the gel beads and the tracer, defined in three dimensions as [170]

$$G_{\text{tg}}(r, \Delta) = \frac{C^{-1}}{N} \sum_{i=1}^N \frac{\int_0^{T-\Delta} dt \sum_{j=1}^{N_g} \frac{\delta[|\mathbf{r}_{i,\text{tg}}(t + \Delta) - \mathbf{r}_{i,\text{tg}}(t)| - r]}{4\pi r^2}}{T - \Delta}. \quad (33)$$

Here N_g is the total number of beads in a gel.

In the following, for these quantities we keep the definitions and notations of Ref. [170] where the passive tracer diffusion in a gel network was examined. We emphasize here that for the evaluation of EB (26) and NGP (30) as well as for the displacement-distribution functions G_{tt} and G_{tg} the *time-averaged* characteristics are used. For G_{tt} and G_{tg} , for instance, the averaging is therefore first performed along a single trajectory and then the results are averaged over all available trajectories in the data set.

By caging in the gel due to excluded-volume interactions, a tracer can be trapped in the meshwork for a long time, especially when its diameter exceeds the mesh size and when no network openings emerge (due to, e.g., inflexibility of the bead-to-bead connections). To quantify such trapping events, we compute the PDF of the angles $P(\Theta, \Delta)$ between two consecutive $\Delta/2$ -lagged displacement vectors at time t , where the angle $\Theta_i = \Theta_i(t, t + \frac{\Delta}{2})$ along the i th trajectory of the tracer is defined as

$$\begin{aligned} \cos \Theta_i \left(t, t + \frac{\Delta}{2} \right) &= \frac{[\mathbf{r}_i(t + \frac{\Delta}{2}) - \mathbf{r}_i(t)] \cdot [\mathbf{r}_i(t + \Delta) - \mathbf{r}_i(t + \frac{\Delta}{2})]}{|\mathbf{r}_i(t + \frac{\Delta}{2}) - \mathbf{r}_i(t)| \cdot |\mathbf{r}_i(t + \Delta) - \mathbf{r}_i(t + \frac{\Delta}{2})|}, \end{aligned} \quad (34)$$

and the respective time-averaged PDF reads [212]

$$P(\Theta, \Delta) = \frac{C^{-1}}{N} \sum_{i=1}^N \frac{\int_0^{T-\Delta} dt \delta[|\Theta_i(t, \Delta) - \Theta|]}{T - \Delta}. \quad (35)$$

For a nonhindered isotropic random motion one gets [212]

$$P(\Theta, \Delta) = \frac{1}{2} \sin \Theta, \quad (36)$$

with $0 < \Theta < \pi$, which is peaked at $\Theta = \pi/2$. Deviations in the shape and in the height of this PDF are indicative of caging effects in the network.

4. Distributions of trapping times

To gain a deeper understanding of the transport mechanisms, we also analyze the waiting-time distribution (WTD) of the tracers in a periodic cubic box with the side length $L = 30$. The waiting time is defined here as the temporal interval between the entry time of the tracer into the box and its subsequent escape from it. In virtue of periodic boundary conditions, both the escape and entrance events are treated the same in this context. The density of the WTD (indicated by subscript w) is denoted as $P(\tau_w)$, with $\int_0^\infty d\tau_w P(\tau_w) = 1$. The first moment of $P(\tau_w)$ is the average time a tracer waits before escaping,

$$\langle \tau_w \rangle = \int_0^\infty d\tau_w \tau_w P(\tau_w). \quad (37)$$

The variance related to $P(\tau_w)$ is calculated as

$$\text{Var}(\tau_w) = \langle \tau_w^2 \rangle - \langle \tau_w \rangle^2. \quad (38)$$

We measure the deviation from the mean using the COV defined as [213]

$$\text{COV}(\tau_w) = \sqrt{\text{Var}(\tau_w)} / \langle \tau_w \rangle. \quad (39)$$

As $\text{COV}=1$ for an exponential PDF, any departure from unity indicates a nonexponential nature of the observed WTD. Generally, a higher COV value suggests a larger spread of the observed waiting times.

For a more comprehensive examination of timescales, one can also compute the so-called uniformity index (UI) [213] β defined for two random waiting times τ_1 and τ_2 as

$$\beta = \frac{\tau_1}{\tau_1 + \tau_2}, \quad (40)$$

with β ranging between 0 and 1. The distribution of values of β can be expressed as [213]

$$P(\beta) = \frac{1}{1 - \beta^2} \int_0^\infty \tau_0 P(\tau_0) P\left(\frac{\beta \tau_0}{1 - \beta}\right) d\tau_0. \quad (41)$$

If the ratio of the values of τ_1 and τ_2 is significant, then one expects β to be close to 0 or close to 1. In such a case, τ_w may be dictated by two well-separated timescales and thus the distribution $P(\beta)$ is peaked around 0 or 1. In the opposite scenario, at $(\tau_1 - \tau_2) \approx 0$ the parameter β should have a value of about 1/2. Therefore, the dynamics is expected to be governed by a single timescale, turning the distribution $P(\beta)$ unimodal with a peak at $\beta \approx 1/2$ [213].

III. RESULTS

Here, we examine the dynamics of active tracers in a responsive gellike network via studying the statistical quantifiers from Sec. II E. We start via presenting the results for the TAMSD and its scaling exponent in Sec. III A, then we illustrate and discuss (i) the findings for the higher moments of displacements of the tracers in terms of EB and NGP (Sec. III C), (ii) the outcomes of computer simulations for the WTDs (Sec. III E), and, finally, (iii) the distribution of the UI parameter β (Sec. III F). All the results below are presented systematically for the models of AOUPs and of RTPs, in order to compare and contrast their respective characteristics.

A. TAMSD and its exponent

In Fig. 12 we illustrate how the overall shape of 3D trajectories of the AOUPs evolves upon variation of the tracer activity. Namely, at $\text{Pe} = 0$ no activity is present, and, as per Eq. (7), the recorded trajectory is reminiscent of a nondirected random walk; see Fig. 12(a). For larger activity values, the trajectories start adapting a directional appearance characteristic of superdiffusive [21,22] or persistent walks [214,215]; see Figs. 12(b) and 12(c).

The results of the analysis of simulation data for the mean TAMSD and its scaling exponent for the AOUPs are presented in Figs. 2(a) and 2(b), respectively. The mean TAMSD is computed via double averaging of the tracer positions along each trajectory and among all 15 available trajectories. We

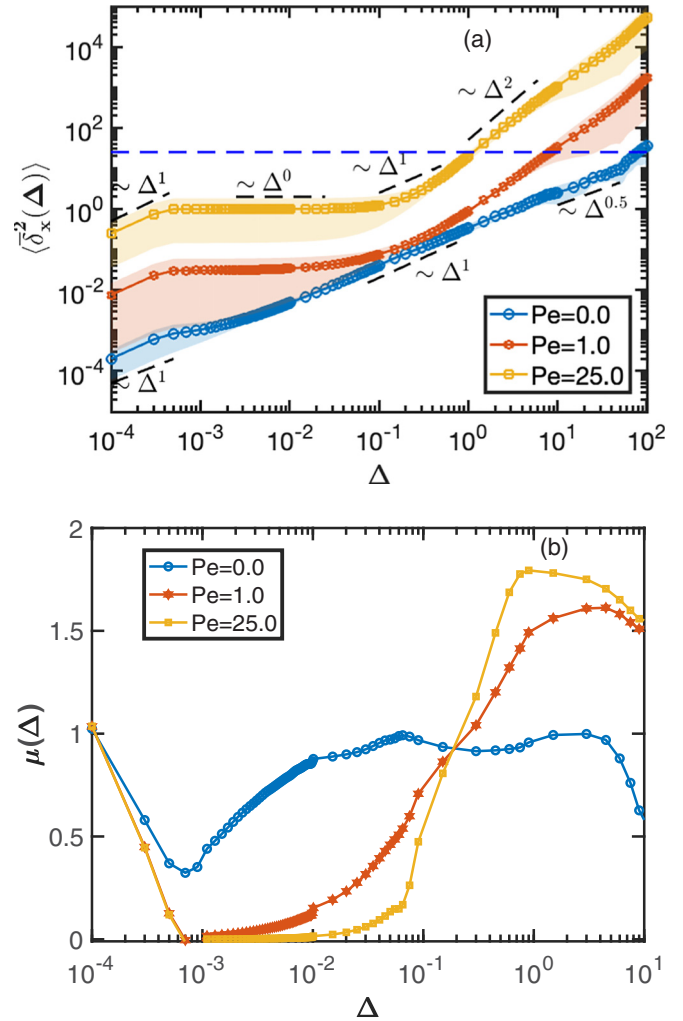


FIG. 2. Diffusion characteristics of AOUPs. (a) Log-log plot of the mean TAMSD $\langle \delta_x^2(\Delta) \rangle$ for different values of the Péclet number (see the legend). The dashed lines shown in panel (a) indicate the slopes of ballistic ($\mu = 2$), of Brownian ($\mu = 1$), of subdiffusive ($\mu = 1/2$), and of confined ($\mu = 0$) motion in terms of the TAMSD evolution (to be used as guides to the eye). The standard deviations for the computed mean TAMSDs are represented by the shaded areas, arising from ensemble averaging. The asymmetry in this area around the mean in panel (a) is due to the log scale. (b) Evolution of the lag-time-local exponent $\mu_x = \mu(\Delta)$ of $\langle \delta_x^2(\Delta) \rangle$ given via Eq. (25), also shown in log-log scale, but only up to $\Delta = 10$. Parameters: the size of the tracer is $\sigma_\tau = 5$, the persistence time of the dynamics is $\tau_{\text{act}} = 5$, the total trajectory length is $T = 5 \times 10^2$, and averaging is performed over $N = 15$ trajectories of the tracer. The horizontal dashed blue line in panel (a) indicates the value of the square of the cell size.

compute below the TAMSDs (20) and (21) only—and not the MSD—because of a rather small and limited number of very long trajectories available from simulations. Although we only present here the results for a single-coordinate TAMSD component, the findings for the other two components are statistically identical due to isotropic diffusion and the cubic symmetry of the elastic network. The time-local scaling exponent of the mean TAMSD in Fig. 2(b) is computed via Eq. (25) with the use of $n_{\text{fit}} = 10$ points of the TAMSD trajectory

(this number is a parameter and can quantitatively affect the obtained values of the diffusion exponents and of the transport coefficients, see the discussion in Refs. [157,216,217]). Note also that the analysis of the ensemble-average MSD would give rise to large inaccuracies due to small-sample-size-induced fluctuations of the computed mean, as given by

$$\langle x^2(t) \rangle = N^{-1} \sum_{j=1}^N x^2_j(t) \approx \int x^2 p(x, t) dx. \quad (42)$$

Therefore, we restrict ourselves here to the TAMSD-based analysis, based on very long trajectories.

As a reference, a prior investigation of passive diffusion of tracers in similarly constructed gels reported in Ref. [170] revealed an initially diffusive behavior at $\Delta \lesssim 10^{-2}$, with a transition to a subdiffusive TAMSD growth at intermediate lag times. Naturally, the TAMSD exponent was found in Ref. [170] to decrease in this second subdiffusive regime for progressively larger—and thus increasingly more confined—tracers, namely, from $\mu \approx 0.9$ down to $\mu \approx 0.4$.

Our simulations of the passive tracers at $Pe = 0$ give rise to a rather small magnitude of the mean TAMSD and to a slightly subdiffusive dynamics across almost the entire range of lag times; see Fig. 2. As expected, with increasing Pe numbers (indicative of enhanced activity of the tracers) the mean-TAMSD magnitudes grow, as compared to those for passive diffusion. Additionally, for active tracers we observe a very short initial regime ($\Delta \ll 10^{-3}$) of nearly Brownian behavior followed by *strongly subdiffusive* behavior. Specifically, at short lag times (at $\Delta \sim 10^{-3}, \dots, 10^{-2}$) the anomalous exponent quickly drops and we find very small values of $\mu \approx 0$, indicative of a transient caging of active tracers.

The emergence of this short-time subdiffusion can be explained by confinement of active tracers within a meshwork, both due to caging effects and directional bias [187,218]. At $t \ll \tau_{act}$ the self-propulsion force maintains a nearly constant direction, entrapping the tracers temporarily in the meshwork of periodically positioned beads (see the video files in the SM). A stronger confinement is typically experienced at higher activities. At longer times (when $t \gg \tau_{act}$) the tracers can freely reorient themselves and break through this activity-induced “blockade.” With increasing activity, the tracers can overcome the energy barriers imposed by cage restrictions more easily. Eventually, as the tracers are released from their cages, a highly directed motion is observed, leading to superdiffusion at intermediate lag times; see Figs. 2(a) and 2(b). The time of onset onto a superdiffusive behavior coincides with the decay of the average persistence of the self-propulsion force. Hence, at higher τ_{act} values the transition to superdiffusion occurs at longer times, as illustrated in Figs. 13(a) and 13(b).

This strongly subdiffusive regime is succeeded at lag times $\Delta \sim 10^{-2}, \dots, 10^0$ by a crossover to a *superdiffusive* behavior observed at $\Delta \sim 10^0, \dots, 10^2$, with the TAMSD exponent $\mu \approx 1.6$. This means that a persistent close-to-ballistic anomalous scaling exponent is observed for the mean TAMSD at intermediate-to-long times ($\mu \sim 1.5, \dots, 2.0$). The spread of individual TAMSDs (used to compute the mean TAMSDs of AOUPs presented in Fig. 2) are plotted in Fig. 14.

We also examined the evolution of the mean TAMSD of AOUPs at a specific Pe value ($Pe = 1$) and for varying times of the directional persistence τ_{act} , see the results presented in Fig. 13. As anticipated, the magnitude of the mean TAMSD increases for longer persistence times of the tracers [Fig. 13(a)], while the local TAMSD scaling exhibits an S-shaped or sigmoidal variation with the lag time Δ , as depicted in Fig. 13(b).

Notably, superdiffusive behavior is observed predominantly at longer lag times as the persistence time increases. In this regime, the scaling exponent of the mean TAMSD increases with increasing τ_{act} ; see Fig. 13(b). For larger values of τ_{act} the superdiffusive behavior characterized by $1.5 < \mu \leq 2$ is shifted to longer lag times. Specifically, the highest value of the exponent μ is observed at $\Delta \gtrsim \tau_{act}$. This peak value of μ becomes more pronounced for larger τ_{act} values. Conversely, the minimum value of μ during the subdiffusive regime is at its lowest for the same cases. Note that a comparable S-shaped variation of μ was previously also reported for the diffusion of an active tracer in dense glass-forming suspensions [84] and for the diffusion of a passive tracer in a medium containing active hard disks [219].

We thus find that for AOUPs, the mean-TAMSD evolution exhibits several distinct regimes of dynamics across different regions of the lag time. Initially, the dynamics are diffusive. Subsequently, the TAMSD follows $\langle \delta^2(\Delta) \rangle \propto \Delta^\mu$, where $\mu \gtrsim 0.5$, within the lag-time range $\Delta \sim 10^{-3}, \dots, 10^{-2}$. Following this regime, our simulations reveal a prominent superdiffusive behavior with μ in the range $1.5, \dots, 2$. The variation of the local scaling exponent (25) with the lag time is less trivially connected to the Pe numbers; see Fig. 2(b). While for intermediate lag times, the exponent μ of the tracer trajectories with large Pe number is the largest, the situation for short lag time is the opposite. At very long lag times, the exponent μ likely tends to approach unity, indicative of BM. This long-time behavior is expected physically because at long times—after a larger number of alternations of the directions of motion—the tracer should diffuse normally, but with a renormalized diffusion coefficient. Certain irregularities in the values of μ observed at very long lag times stem from unavoidable deficiencies in the TAMSD averaging statistics, which are also present for conventional BM [22].

The standard deviations around the mean TAMSD for the passive-tracers case computed from the data are shown in Figs. 2(a) and 13(a). These can be reduced via averaging over the two other (independent) directions of diffusion (y and z) as well as via increasing the number of statistically independent trajectories in the data set. For the same number of trajectories used for averaging, for diffusion of active tracers the standard deviations are generally larger, compare their magnitudes in Figs. 2(a) and 13(a). For the situation considered, the standard deviations decrease at intermediate lag times, as also supported by a shrinkage of the distribution of individual TAMSDs in this region (a more reproducible motion); see Fig. 14. Finally, the inaccuracies in the determination of the mean TAMSD naturally increase towards the end of the recorded trajectories (for this and many other stochastic processes) because of worsening statistics of sliding-window-based averaging [22,157].

B. Amplitude spread of the TAMSDs

In Figs. 14 and 15 we illustrate—for AOUPs and for RTPs, respectively,—the variation of the values of individual TAMSDs at varying activities over the entire range of lag times. For AOUPs, the PDFs $p(\xi_x(\Delta))$ are depicted in Fig. 16 and in Fig. 17 for RTPs. For passive tracers, the distribution $p(\xi_x(\Delta))$ is unimodal, exhibiting a pronounced peak at $\xi_x = 1$ at all lag times; see Fig. 16(a). As the lag time increases, the distribution broadens significantly. In contrast, for AOUPs, the distribution becomes bimodal, with two distinct maxima and a minimum around $\xi_x \approx 1$. At both shorter and longer lag times, the bimodal distribution $p(\xi_x(\Delta))$ becomes slightly skewed to the left or right, as shown in Figs. 16(b) and 16(c). At intermediate lag times, the PDF remains bimodal, but the spread of the respective distribution is reduced. This emergence of bimodal PDFs at nonzero activities of the particles indicates their splitting into two “nonoverlapping” subpopulations.

For RTPs, the TAMSD distribution $p(\xi_x)$ is evidently much more localized, with the spread of TAMSDs being particularly small at large Péclet numbers; see the $Pe = 25$ data in Figs. 3 and 17(c). At $Pe = 1$, the distribution $p(\xi_x)$ exhibits a unimodal behavior around $\xi_x = 1$, slightly skewed to the right; see Fig. 17(a). At a high activity ($Pe = 25$), the distribution is unimodal, featuring a very sharp peak precisely at $\xi_x = 1$; see Fig. 17(c). The latter is indicative of extreme reproducibility of individual TAMSDs and ergodicity of the dynamics of RTPs in this regime of model parameters. Note that, in contrast to the AOUPs, the RTPs can move only in a restricted direction, allowing it to explore only specific spaces. Therefore, the dynamics of RTPs in the x -direction is less influenced by movements in the other two directions. This can be envisaged via comparing Eq. (5) governing the dynamics of AOUPs and Eq. (8) characterizing the RTPs.

C. EB and NGP

Upon examining the distributions of the TAMSD spreads presented in Figs. 14 and 15, we compare the EB parameter $EB(\Delta)$ for AOUPs to that for RTPs via presenting the EB results in Figs. 4(a) and 4(b), respectively. In correspondence to a much smaller spread of the TAMSDs for RTPs, the respective EB parameters (particularly at higher Pe numbers) are considerably smaller, as compared to the case of AOUPs. For the latter we observe a weakly nonergodic behavior, with the scatter of the TAMSDs variation displaying a *nonmonotonic* trend with activity of the particles, notably showcasing a minimal spread of the recorded TAMSDs at intermediate values of Pe (in this case, $Pe = 1.0$); see Fig. 4(a). This nonmonotonicity is also visible from the original TAMSD distribution in Fig. 14. An increase of EB at very long lag times can be attributed to statistical inaccuracies of the TAMSD evaluation, known to occur also for other underlying stochastic process.

In contrast, for RTPs we observe that the spreads of the TAMSDs becomes smaller than those of passive motion and they decrease with progressively higher tracer activity, as illustrated in Figs. 16 and 17. At higher Pe values, the system approaches a much more ergodic behavior, with very small EB values, as quantified in Fig. 4(b). Note that both for AOUPs and for RTPs we find that the EB is not a linearly increasing

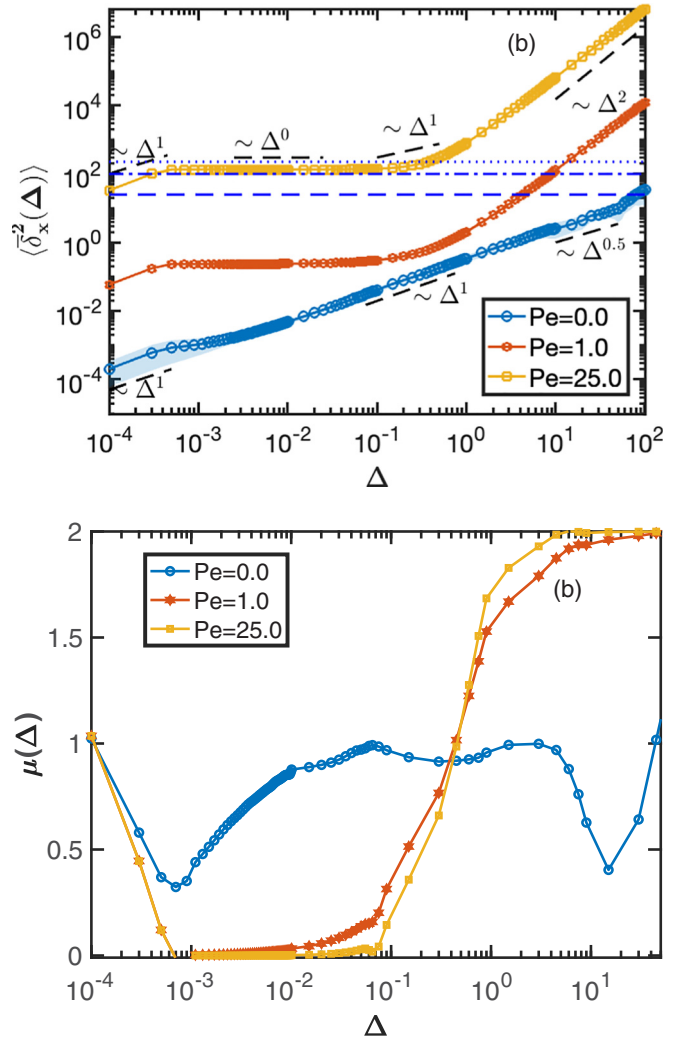


FIG. 3. The same quantities as in Fig. 2, but computed for RTPs diffusing in gels. Parameters: $\sigma_t = 5$, the Poissonian rate is $r_0 = 1$, $T = 500$, and $N = 15$. The horizontal lines in panel (a) correspond to the magnitudes of the squares of one, two, and three cell sizes.

function of the lag time. Such a linear dependence is known for conventional BM [22], where the dependence (27) is valid. For AOUPs and RTPs, in contrast, the EB parameter varies somewhat, but does not reveal a tendency to grow as a power law at longer lag times.

The NGP parameter $\gamma_x(\Delta)$ defined by (30)—computed from the results of our simulations and shown in Fig. 5—demonstrates a decaying behavior with the lag time. At very short lag times (of the order of a simulation time step) large values of γ_x were found. Note that, unlike some previous investigations [177,179], the tracers in our study are not initially at equilibrium or in a steady state with the gel network. As the lag time increases, we thus find that the NGP $\gamma_x(\Delta)$ gradually reduces to unity indicating a Gaussian behavior of the respective PDFs. Note that both for AOUPs and for RTPs, the value of $\gamma_x(\Delta)$ significantly increases as we go from lag times $\Delta \sim 10^0$ to $\Delta \sim 10^{-2}$, especially in situations of high tracer activity. This finding strongly indicates the presence of a pronounced non-Gaussian dynamics of tracer

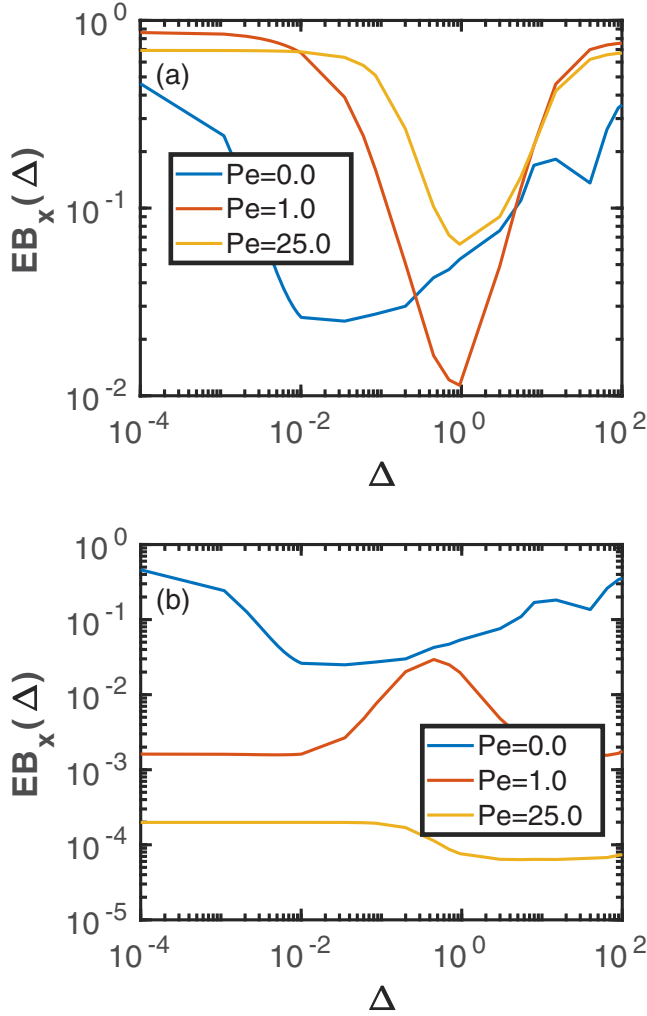


FIG. 4. EB parameter (26) as a function of Δ computed as the squared coefficient of variation from the TAMSDs of AOUPs shown in Fig. 2(a) and of RTPs shown in Fig. 3(b) for different Pe numbers (see the legend), shown for the same respective model parameters.

displacements at short and a crossover to a Gaussian dynamics at long lag times Δ .

D. Displacement-distribution functions

We analyze the tracer-tracer self-HCFs $G_{tt}(\chi, \Delta)$, as shown in Figs. 6 and 7 for AOUPs and RTPs, respectively, for several values of the lag time. As most of the PDFs are symmetric functions (except for those in Figs. 7(e) and 7(f)), only the region of positive displacements are shown in Figs. 6 and 7. At short lag times, the distributions of the tracers can be approximated by *compressed Gaussian* functions in the central region of small displacements. Namely, in Figs. 6(a)–6(c), the simulation data are fitted with

$$G_{tt}(\chi) \propto \exp(-[|\chi|/a_{0,\eta}]^\eta). \quad (43)$$

For $Pe = \{0, 1, 25\}$, the values of the scale parameter $a_{0,\eta}$ and of the exponent η are determined by fitting to be $a_{0,\eta} \approx \{1.1827, 1.1718, 1.1323\}$ and $\eta = \{2.5587, 2.5388, 2.4223\}$,

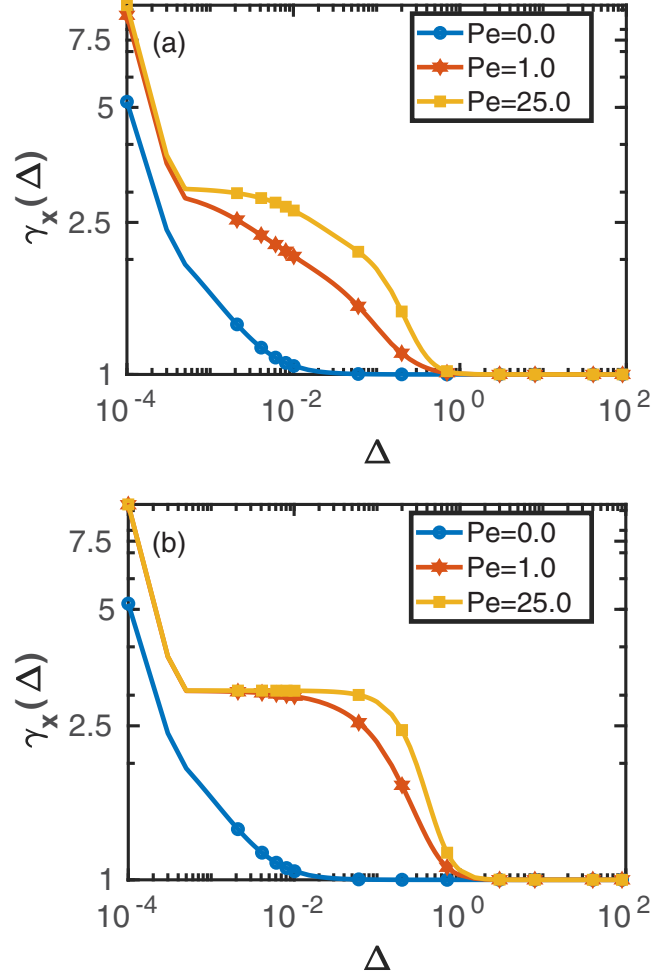


FIG. 5. NGP γ_x given by Eq. (30) as a function of the lag time Δ in log-log scale computed for the dynamics of AOUPs (a) and of RTPs (b), computed for the respective parameters of Fig. 2 and of Fig. 3.

respectively. Here and below, the distances such as $a_{0,\eta}$, χ , and r are provided in units of σ_g ; see Table I.

At long lag times, of Figs. 6(d)–6(f) showcase fits to the data using the *Gaussian* functions of the form

$$G_{tt}(\chi) \propto \exp[-\chi^2/(2a_{0,2}^2)], \quad (44)$$

where for $Pe = \{0, 1, 25\}$ the values of the standard deviation $a_{0,2}$ are found to be $a_{0,2} \approx \{1.0004, 1.0040, 1.1048\}$, respectively. The so-called “full width at the half maximum” for the function $G_{tt}(\chi)$ is calculated for $Pe = \{0, 1, 25\}$ to be $\approx \{2.3557, 2.3643, 2.6016\}$, respectively.

We thus demonstrate that as the lag time increases the PDFs of the displacements of the tracers change their form from a compressed Gaussian (43) to a Gaussian (44). We note that some fluctuating tails of the displacement distributions observed here are the results of numerical inaccuracies found at very small values of the PDFs in Figs. 6 and 7. Similar features were observed earlier in Refs. [177,179] for tracer diffusion in a polymer network.

We find that with increasing activity of the particles, the central peak of the distribution functions broadens, and the

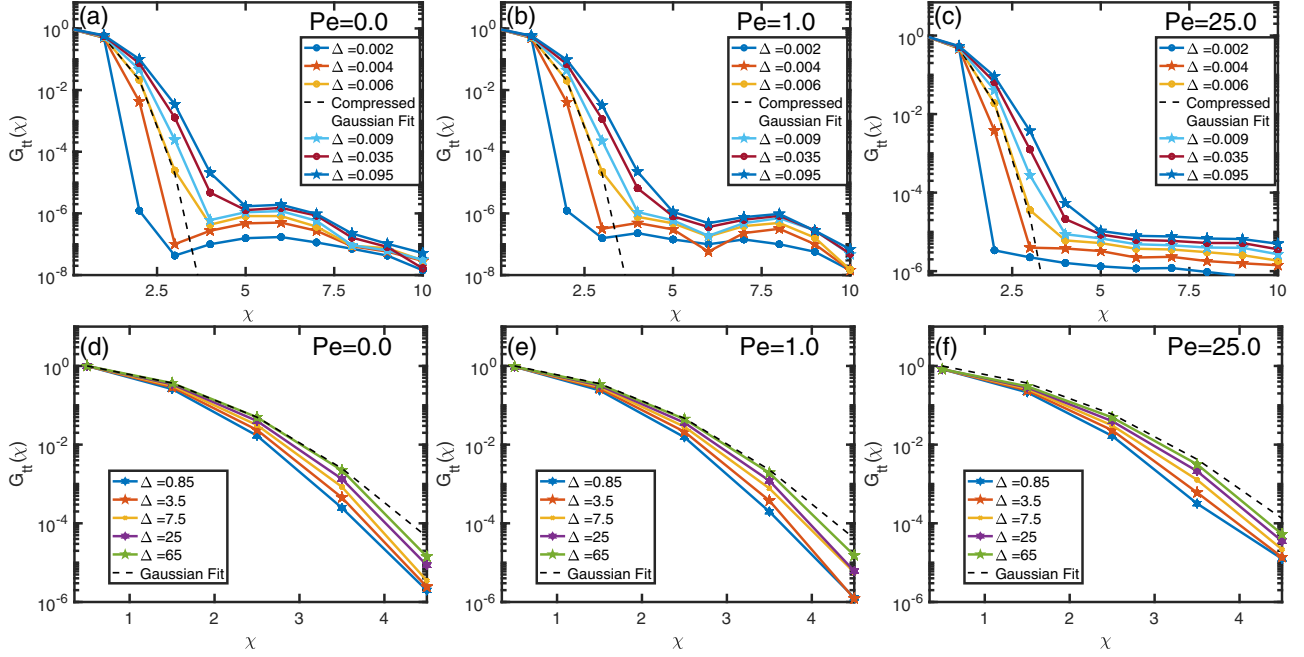


FIG. 6. Self-HCFs given by Eq. (31) plotted as a function of displacement χ (in units of σ_g) of AOUps at short (a)–(c) and long (d)–(f) lag times (see the legend for exact values) for varying activities of the particles. The dashed lines represent the analytical functional dependencies (43) and (44) as fits to the obtained simulation data at $\Delta = 0.006$ and $\Delta = 65$ (see the main text for the values of the fit parameters). All other parameters are the same as in Fig. 2.

tails of the distribution become smoother. At longer lag times, the distribution becomes approximately Gaussian with an elevated standard deviation at higher Pe values, see the respective panels in Figs. 6 and 7. In Fig. 7 the dashed lines correspond to expressions (43) and (44) for the *compressed or stretched* Gaussian and Gaussian forms fitting the data obtained from simulations. In Figs. 7(a)–7(c), the values of a_0 used for

fitting are $a_{0,\eta} \approx \{1.1827, 1.1495, 0.5294\}$ and exponents are $\eta = \{2.5587, 2.4979, 1.5468\}$ for $Pe = \{0, 1, 25\}$, respectively. In Figs. 7(d)–7(f), the values of $a_{0,2}$ for the situations $Pe = \{0, 1, 25\}$ were found to be $a_{0,2} \approx \{1.0004, 1.0120, 1.1421\}$, respectively. For the same set of Pe values, the full widths at half maxima are $\approx \{2.3557, 2.3831, 2.6893\}$. To compare, for a perfectly Gaussian PDF, the full

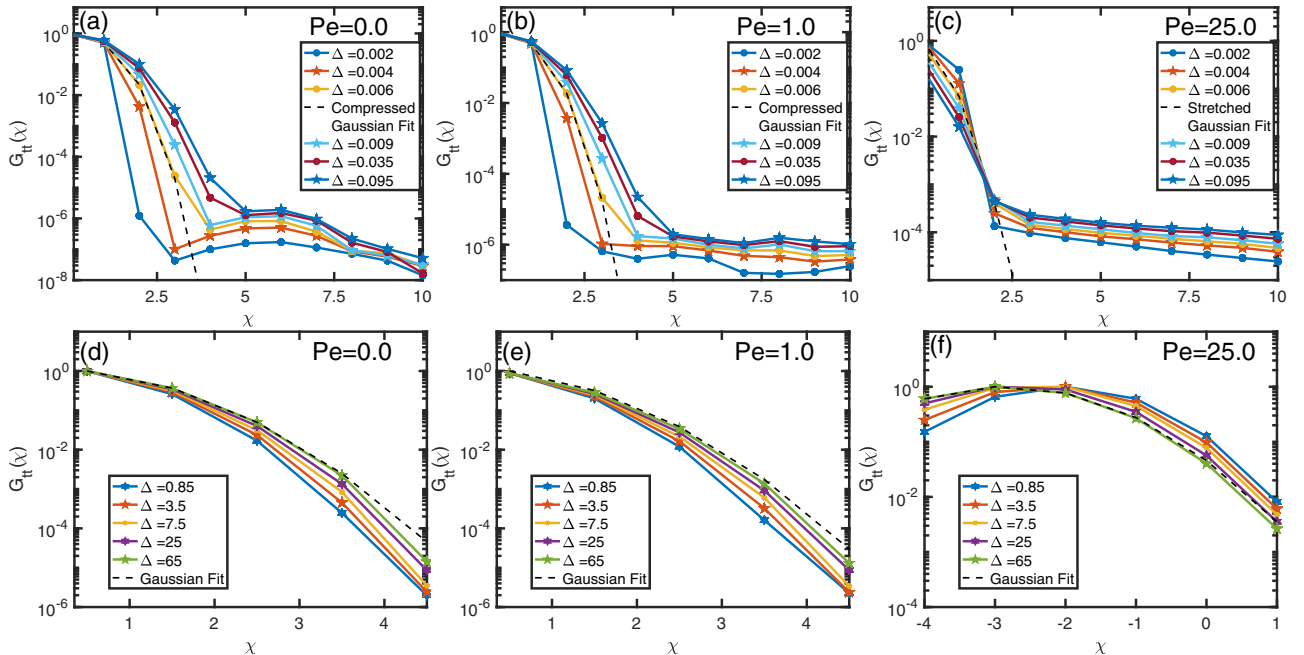


FIG. 7. The same as in Fig. 6, but obtained from simulations of RTPs. The dashed curves are the compressed or stretched Gaussian (43) (see the main text for actual parameters) and the Gaussian (44) distributions. All other parameters are the same as in Fig. 3.

width at half maximum is ≈ 2.355 of its standard deviations.

Note that, except for highly active RTPs, the computed displacement distributions are almost symmetric and feature a zero mean, suggesting an isotropic nature of diffusion at long times. However, in the case of very active RTPs, a mean of the distribution is attained at $\chi < 0$; see Fig. 7(f). This fact can be attributed to the initial drift of the particles acquired via the active force, which initially has negative values in all directions, as mentioned in Sec. II B and shown in Fig. 10. This is not an artifact of a data-sampling method. This asymmetric behavior is also reflected in some distributions of the angles; see, e.g., Fig. 18(e).

Figure 18 illustrates the distributions of angles of AOUPs and of RTPs for a number of lag times. At longer lag times, the distribution is found to be symmetric and to take the form (36), indicative of the expected isotropic diffusion. However, at short lag times, the distribution is found to peak at $\Theta = \pi/2$ that clearly reveals some local heterogeneity. This observation supports the non-Gaussian short-time displacement distribution depicted in Figs. 6 and 7. Interestingly, in the case of RTPs with high activity (at $Pe = 25$), the angle distribution is found to be skewed or asymmetric and also to shift towards the $\Theta < \pi/2$ region at time $\Delta \gtrsim 0.65$. This suggests anisotropic diffusion of the tracers at such conditions.

We analyze now the radial distribution $4\pi\chi^2 G_{\text{tr}}(\chi, \Delta)$ given by (31) and the cross-HCFs $G_{\text{tg}}(\chi, \Delta)$ given by (33) at different lag times for different activities of the particles corresponding to $Pe = \{0, 1, 10\}$, as depicted in Figs. 19–22. Figures 19 and 20 illustrate the computed PDFs defined by Eq. (32) along the radial distance r for AOUPs and RTPs, respectively. At short lag times (at $\Delta \lesssim 0.1$), the maximum of the displacement function of the tracers $4\pi\chi^2 G_{\text{tr}}(\chi)$ is found at a distance $r \lesssim 2.5$. Furthermore, the likelihood of finding a tracer beyond the gel mesh size of $r \approx 5$ is vanishingly small, indicating a predominant confinement within a single mesh. At longer lag times, the maximum probability for the AOUPs is centered at around $r \approx 2.5$, suggesting some fluctuations of the lattice around the mean position within a cell of the network. The distance of $r \approx 2.5$ corresponds to a half of the mesh size: such tracers are thus located at the center of the respective cells. At higher activity of the particles (at $Pe = 25$), we find an increased occurrence probability of the AOUPs and of RTPs at distances beyond $r = 5$, as depicted in Fig. 19(f) and most pronouncedly in Fig. 20(d), correspondingly.

This suggests that—although the tracers are most likely confined to a single cell of the mesh—a movement to one of the neighboring sites increases over time for conditions of higher activity. Note also that, especially in the case of RTPs, the maximal probability occurs at $r \approx 5.0$, and the relative displacement shifts towards distances $r > 5.0$. This could be due to the initial drift of such active tracers, which makes them likely to escape the initial site and to diffuse to a neighboring site of the network, as discussed earlier. The effect of diffusion from one site of the network to the next due to the so-called “cage opening” is clearly visible for highly active particles at long times; see Fig. 19(f) for AOUPs and especially Fig. 20(d) for RTPs, as well as the discussion below.

Figures 21 and 22 depict the cross-HCFs G_{tg} between the gel beads and the tracers, represented by AOUPs and by RTPs,

respectively. In all the cases, a distinct peak is evident at the trace-bead separation of $r \approx 3$ (r is measured in units of σ_g), corresponding to the beads in the first cell around the tracer. In the case of a passive tracer, illustrated in Fig. 21(a), there are some minor peaks also beyond the threshold value of $r \approx 3$. The distance of $r \approx 3$ in the tracer-gel correlation refers to the average distance between the tracer and the nearest gel bead given by Eq. (16). The first peak broadens and shifts towards larger r values at lag time $0.1 \lesssim \Delta \lesssim 1$, indicating free diffusion of the tracer due to gel-tracer collective fluctuations. At longer lag times, peaks near $r \rightarrow 0$ suggest exceedingly larger fluctuations of the tracer. At higher Pe values, a pronounced first peak at short lag times $\Delta \lesssim 0.1$ is observed, indicating the strong confinement of the tracer within the mesh due to the negative viscoelastic response of the gel network to the tracer motion. This observation is corroborated in Figs. 2 and 3. However, at intermediate-to-long lag times and at higher Pe values the first peak shifts towards comparatively larger r values in Fig. 19(f), which is a signature of cooperative gel-tracer motion indicative of cage-opening events.

E. WTDs

The escape dynamics of SPPs from confined domains has been previously studied; see, e.g., Refs. [220–223]. Below, we analyze the waiting time of the tracers between two successive escape events from a cell in the periodic gel network of volume $L \times L \times L = 30 \times 30 \times 30$ (in units of the mesh size). In the simulations, we monitor the number of steps n_w taken by a tracer to either exit or to reenter the defined domain. Employing periodic boundary conditions, we designate the act of entering into or of escaping a certain spatial domain as an “event.” The time instance of such an event is determined by multiplying the step count n_w by the time increment Δt in our simulations. The time difference between the occurrences of two sequential events is defined as the waiting time, denoted here as τ_w , and the PDF of these times (named WTD) is extracted from the simulation data.

The WTDs $P(\tau_w)$ are plotted for various values of Péclet number in Figs. 23 and 24 for the case of AOUPs and of RTPs, respectively. These results reveal that the WTDs deviate from a single-exponential behavior at low tracer activities. In the case of AOUPs, the WTD initially follows an exponential decay law with a short timescale over a limited range of waiting times; see Fig. 23. Notably, some outliers occur in the long tail of the WTD: this tail at later times can be fitted with another exponential function having a much longer timescale, as compared to the initial one. As the value of Pe increases [see the legends of Figs. 23(a)–23(d)], this second timescale becomes gradually and dramatically shorter. Eventually, at very high Pe values [see Fig. 23(d)], the WTD is excellently described by a single-exponential decay,

$$P(\tau_w) = \langle \tau_w \rangle_f^{-1} \exp[-\tau_w / \langle \tau_w \rangle_f], \quad (45)$$

with the characteristic time $\langle \tau_w \rangle_f$. Upon fitting the simulation data, we determined that this scale is $\langle \tau_w \rangle_f \approx 2.65$, which closely approximates the mean waiting time $\langle \tau_w \rangle \approx 2.73$ obtained from the simulation data [see Fig. 23(d)]. This fact supports the exponential form (45).

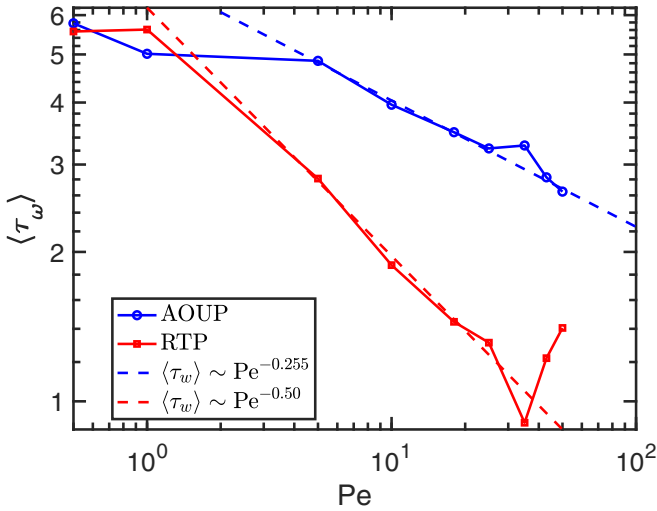


FIG. 8. Log-log plot of the mean waiting time as a function of Péclet number for the case of AOUPs and of RTPs, as indicated. The dashed lines are the asymptotes provided in the legend.

For the case of RTPs, the distribution cannot be accurately fitted with any exponential function across the domain of examined Pe values, as illustrated in Fig. 24. At intermediate Pe values, with Pe in a range from ≈ 10 to ≈ 25 , a plateau-like behavior is observed at short times. However, at Pe = 50 some outliers emerge at later times, extending beyond the range of exponential fitting and rendering the distribution nonexponential.

The mean waiting times $\langle \tau_w \rangle$ of the respective WTDs as well as their fluctuations quantified by the respective COVs are presented in Figs. 8 and 9, respectively. The times $\langle \tau_w \rangle$ exhibit distinct characteristics across various ranges of Pe values for both AOUPs and RTPs, as depicted in Fig. 8. Specifically, for Pe $\lesssim 5$ in the case of AOUPs and for Pe $\lesssim 1$ for the case

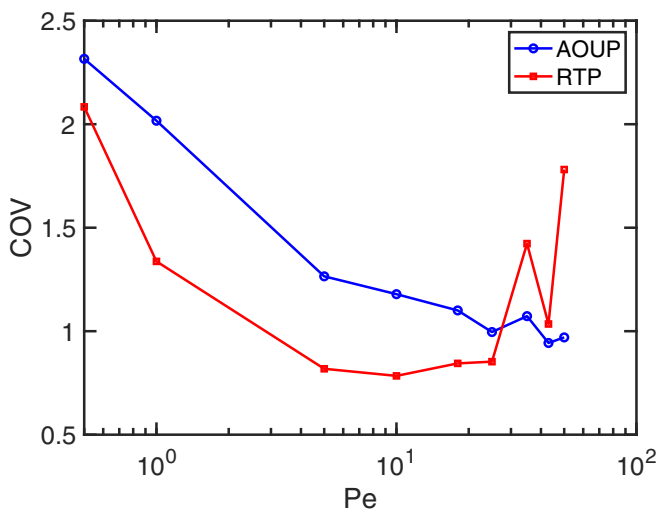


FIG. 9. COV of the WTDs plotted versus the Péclet number in log-lin scale for the case of diffusion of AOUPs and of RTPs, as indicated. For large Pe numbers, the COV approaches approx. unity for the WTDs of AOUPs, whereas it exhibits a nonmonotonic and fluctuating dependence on Pe for the case of RTPs.

of RTPs, the mean shows a slight dependence on Pe number. Beyond Pe $\gtrsim 5$ and Pe $\gtrsim 1$ regions, respectively, the waiting time decreases monotonically and significantly with Pe, up to Pe = 25. This variation can be effectively described by a power-law dependence

$$\langle \tau_w \rangle \sim Pe^{-\alpha}, \quad (46)$$

for the exponent of which we find $\alpha \approx 0.255$ for AOUPs and $\alpha \approx 0.5$ for RTPs. In the case of AOUPs, in the activity region beyond Pe = 25, $\langle \tau_w \rangle$ exhibits a decay with Pe, displaying a slight nonmonotonic behavior (within the margin of numerical error).

Conversely, for RTPs, there is a pronounced nonmonotonic behavior in the variation of the mean waiting time at large Pe values (see Fig. 8): specifically, after a certain Pe number the mean waiting time starts to grow. The observed power-law behavior at intermediate Pe aligns with the previous findings of Ref. [177]. This behavior can be attributed to an increased dynamics associated with higher activity, resulting in tracers exploring the simulation box in shorter average times. In the case of RTPs, for which motion of the tracers is directed along specific directions, higher activity implies faster exploration over larger length scales, leading to a significant decrease in the computed mean waiting time; see Fig. 8.

Figure 9 illustrates that the COV for the case of AOUPs decreases nearly monotonically, approaching \approx unity at higher activities of the particles. This observation supports the exponential behavior of the WTDs at large Pe values for AOUPs (see Fig. 23), because COV = 1 for exponential WTD. In contrast, an exponential law is reported for all activities of the tracers diffusing in a flexible gel network in a recent study of Ref. [177]. However, note that the case considered here involves a slightly different gel network and we also define the waiting time differently than the method of Ref. [177].

A nonmonotonic behavior of the COV for the case of RTPs is evident from Fig. 9. Specifically, the COV reaches a minimum (COV < 1) at an intermediate Pe number, and COV increases beyond unity in the high-activity regime. Similar variations of the COV, corresponding to the first-passage time of SPPs confined within a domain, were reported previously in Refs. [220,222]. From Fig. 9 it becomes apparent that the COV is significantly greater than unity for a nearly passive case and that COV $\neq 1$ at low activities. Therefore, this COV variation aligns with the characteristics of the WTDs. The increase of the COV for RTPs at high Pe numbers is mathematically due to the fact that the average time of the WTD PDF obtained from our simulations becomes progressively shorter in this regime [compare Figs. 24(a) and 24(b) with Figs. 24(c) and 24(d)]. Physically, the mean waiting time for RTPs decreases at high Pe due to activity-facilitated, quicker escape of the tracers from their cages in the network. As a result, the COV defined via (39) for RTPs increases at large Pe numbers, as demonstrated in Fig. 9, in contrast to the case of AOUPs, where the COV decreases monotonically with Pe. The COV reaches a minimum for RTPs when the fluctuations of the recorded waiting times around their mean are minimized. For AOUPs, as Pe number increases, both short and long waiting events become similar in duration. In contrast, for RTPs, beyond a certain Pe value, the two types of trajectories become increasingly distinguishable. This yields

a larger dispersion of values around the mean and, consequently, larger COV values at larger Pe numbers for RTPs.

F. UI

Figures 25 and 26 depict the corresponding distributions $P(\beta)$ of the UI, defined as β in Eqs. (40) and (41). The shape of $P(\beta)$ is mainly determined by the sign of the coefficient C_2 in the quadratic polynomial used for fitting,

$$P(\beta) \approx C_2\beta^2 + C_1\beta + C_0. \quad (47)$$

For $C_2 < 0$ or $C_2 = 0$ or $C_2 > 0$ the distribution $P(\beta)$ exhibits a bell-shaped or plateau-like or M-shaped form, respectively. Figure 27 illustrates the variation of C_2 with Pe values. The polynomial (47) corresponds to the fit for the distribution $P(\beta)$ in the domain $0.02 < \beta < 0.98$, and the value of C_2 dictates its shape. If necessary, some of the observed bimodal and single-peaked $P(\beta)$ distributions can also be fitted with two-parameter Beta distributions.

Examining the UI distributions $P(\beta)$ in Figs. 25 and 26 provides deeper insights into the timescales of the escape dynamics of tracers from cavities in the gel meshwork. Let us first consider the case of AOUPs shown in Fig. 25. At low Pe values the distribution exhibits an M-shaped pattern with two peaks at $\beta = 0$ and $\beta = 1$, and with a minimum at $\beta \approx 1/2$. This configuration suggests the presence of two distinct timescales for waiting times. Indeed, the WTDs in this situation are well fitted with double-exponential decay laws, each associated with a distinct timescale [see Figs. 23(a)–23(c)]. As Pe value increases, the magnitude of C_2 gradually decreases, reaching near-zero values in the region $Pe = 20, \dots, 30$. At even higher Pe values, C_2 assumes a slightly negative value, indicating a transition to a single timescale dominating the dynamics of tracers. As previously analyzed in Fig. 23(d), this regime indeed corresponds to a single exponential decay.

For the case of RTPs, the sign of C_2 changes from positive to negative as Pe number increases from $Pe = 0$ to $Pe = 35$. Beyond $Pe = 35$, the variations of this coefficient become nonmonotonic, see Fig. 27, but its value consistently remains negative here. As depicted in Fig. 26, the PDF $P(\beta)$ is bimodal (M-shaped) at small Pe numbers. At intermediate Pe values, the PDF becomes almost flat, with a developing peak around $\beta = 1/2$, as shown in Fig. 26(b). At even higher Pe values, the PDF of escape times transforms into a unimodal (bell-shaped) distribution, with a pronounced single peak at $\beta = 1/2$, suggesting a single timescale dominating the WTD.

Hence, for both AOUPs and RTPs, it is evident from these data that both very short and very long waiting times are observed in our simulations. Short waiting times indicate instances when the tracer promptly exits and reenters the box, potentially encountering hindrance from the meshwork near the box boundary. These rapid fluctuations, leading to shorter trajectories near the boundary, are notably pronounced for tracers solely influenced by thermal noise. In contrast, if the tracer particle initiates near one side of the box and avoids exiting from this side, it requires an extended time to reach any other sides for an exit, especially when the particle's activity is comparatively low (small respective Pe numbers). Consequently, longer tracer trajectories with waiting times $\tau_w = 50, \dots, 150$ are noticeable at low Pe, as shown

in Figs. 23(a) and 23(b). As Pe increases, the length of longer trajectories shortens and it becomes comparable to the shorter ones, resulting in decreasing mean waiting times.

IV. DISCUSSION AND CONCLUSIONS

We studied multiple features of diffusion of activity-driven tracers in a responsive gel network, in particular for situations when the tracer size is comparable to the mesh size of the network. Our main findings based on the results of extensive computer simulations are as follows. (i) A tracer becomes trapped inside a gel at intermediate timescales, leading to a subdiffusive behavior often characterized by a compressed Gaussian distribution. (ii) At long lag times, the particle can escape from the cage, exhibiting superdiffusive spreading behavior in the gel. The distribution of tracer displacements can be described as a Gaussian with enhanced diffusivity. (iii) The motion of AOUPs in gels is a process with weakly nonergodic dynamics, while spreading of RTPs is an almost ergodic process. (iv) The escape of tracers from individual cells of the gel network is governed by two waiting timescales; at higher activity of the tracers, these timescales become comparable. Specifically, for AOUPs at high activity, the waiting times are distributed exponentially with a single timescale. (v) The mean waiting time for the evaluated WTD becomes shorter as the activity increases, particularly following a power-law relationship (46) at intermediate Pe values.

Our results capture a general trend in the diffusion of an active tracer, exhibiting both trapping events (leading to a subdiffusive regime) and activity-driven propagation (giving rise to a superdiffusive regime). For a passive tracer, the dynamical features were shown to be subdiffusive at intermediate times, in agreement with earlier studies of similar systems [170,212]. The caging effect was demonstrated above to be more pronounced for active tracers, as reflected in their individual dynamics as well in the collective motion of the gel beads. Over time, the evolution of the distribution of displacements from a non-Gaussian to a Gaussian one was found, with enhanced diffusivity of active tracers, as intuitively expected.

We present now a short comparative analysis of related results in recent literature. In contrast to Ref. [177], our observations revealed initial subdiffusion due to caging effects, followed by superdiffusion resulting from escape events of active particles from the responsive polymeric-type mesh. Note that we have treated the tracers as massless particles, thus examining their dynamics in the overdamped limit; deviations in the short-time behavior due to effects of inertia are thus possible (see, e.g., Ref. [181] for such effects in massive-particles fractional BM). Also, unlike in Ref. [177], where beads of the gel are connected via short polymeric chains, in our study the beads are directly bonded via the Morse potentials. The dynamical properties associated with an active tracer in our study are akin to those observed in the motion of SPPs in a diamond lattice network [179], in dense glassy systems [84], or in living cells [224].

Let us also briefly discuss now the WTDs. In Ref. [177], the trapping-time distribution of AOUPs in a meshwork was found to be exponential, and the mean time was demonstrated to vary with the particle activity in a power-law fashion at in-

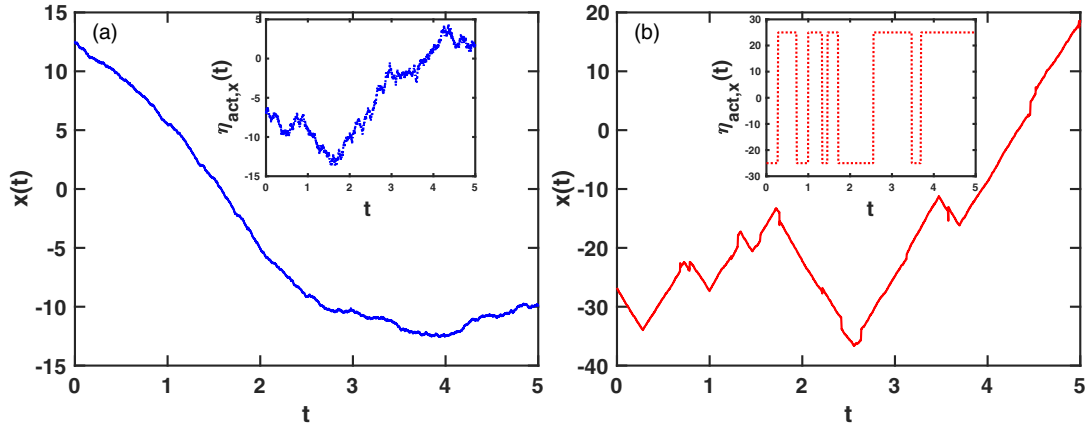


FIG. 10. Trajectories of two types of active particles at $Pe = 25$, diffusing through a meshwork in the x direction, as a function of time t for the case of (a) AOUP and (b) RTP. Insets illustrate the time evolution of respective active noise: for AOUPs the x component of noise varies stochastically, whereas for RTPs the noise alternates between two preset discrete values.

intermediate times. In our study, we examined the WTDs in the context of escape from a periodic gel network, also observing a power-law dependence of the mean waiting time on activity, although with a different exponent. We identified the existence of two time-scales for waiting times, which closely resemble those reported for escape times of SPPs from a confined domain in Refs. [220,222]. At higher Pe -number values, we found the waiting time for AOUPs to follow an exponential distribution, similar to the findings of Ref. [177]. However, the waiting times for the dynamics of RTPs were found to be consistently nonexponential, and their fluctuations around the mean were found to vary nonmonotonically with activity, resembling the observations reported in Refs. [220,222].

Regarding possible applications, the analysis of transport characteristics of active tracers within gellike networks is important in various domains, ranging from medicine to security and environmental sustainability (as outlined with explicit references in Sec. I). This study presents a comprehensive examination of the properties of the diffusion of active tracers, providing insights into the dynamics and into the escape kinetics of two distinct types of active particles, namely AOUPs and RTPs. Our research sheds new light onto similarities and differences in the properties of these types of active particles, enhancing our understanding of their behavior within fluctuating gel matrices.

Further developments and perspectives of this study are multifold. While our primary focus was on the transport of spherical and noninteracting tracers within a gel network, our approaches lay the foundation for extensions to more intricate scenarios. Future investigations may, e.g., explore the transport properties of nonspherical tracers, such as of asymmetric polymersomes commonly employed in controlled drug delivery [225–228]. The diffusion of rodlike particles mimics, e.g., the propagation of single-walled carbon nanotubes in crowded environments [229] or of particles of Tobacco Mosaic Virus [145] in polymeric gels [119]. In these cases, both translational and rotational diffusion [74] of particles are coupled and thus should be examined simultaneously. Furthermore, accounting for diverse physical-chemical close-contact interactions and for variable structures within the gel network,

along with the presence of long-ranged and hydrodynamic interactions, are crucial to fully capture the complexities of active tracer transport in noninert responsive heterogeneous gellike environments.

ACKNOWLEDGMENTS

The authors acknowledge the University of Potsdam for providing access to the supercomputing facility. We acknowledge funding from the German Science Foundation (DFG Grants No. ME 1535/13-1).

APPENDIX: SUPPLEMENTAL FIGURES

Here, we present the auxiliary Figs. 10–27 supporting the claims reported in the main text.

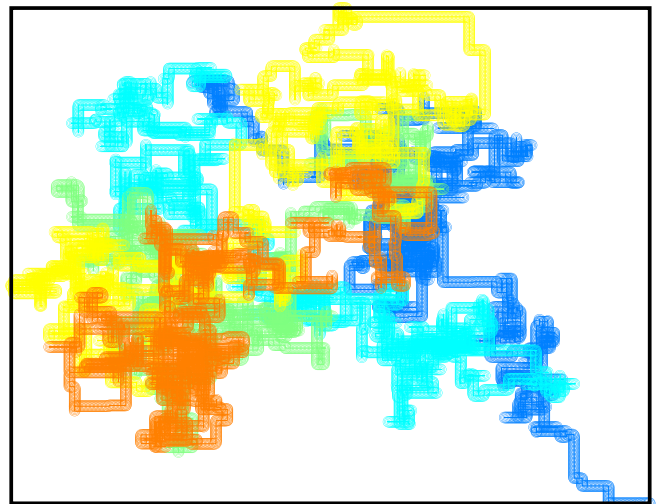


FIG. 11. Sample trajectory of a freely moving 2D RTP, shown in different colors from start (blue) to finish (red). The particle undergoes exploration along four possible directions (left, right, upward, and downward).

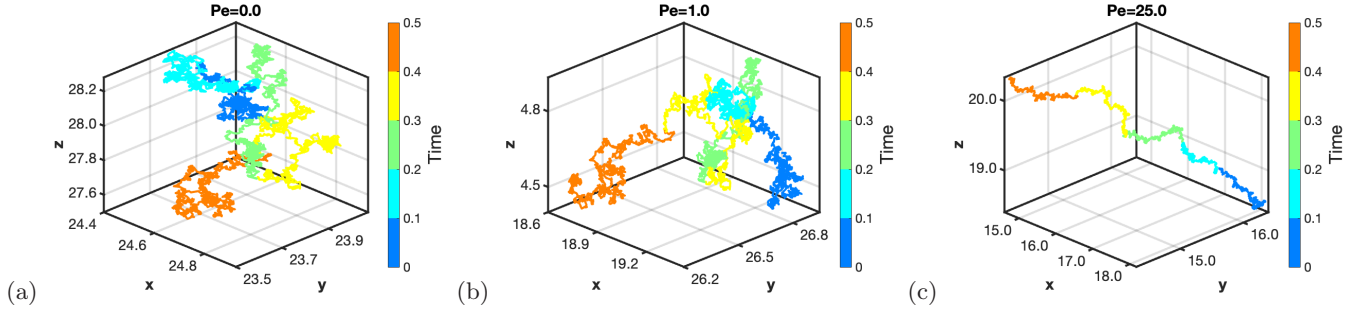


FIG. 12. Typical trajectories of length $N_{\text{steps}} = 5 \times 10^3$ with the time step of $\Delta t = 10^{-4}$ giving the trajectory length (19) of $T = 0.5$ of the dynamics of an AOUP of diameter $\sigma_t = 5.0$ in a gel at three values of the Pe number, as indicated. Varying colors represent the time running from the start to the end of the trajectories (see the color bar in the legend).

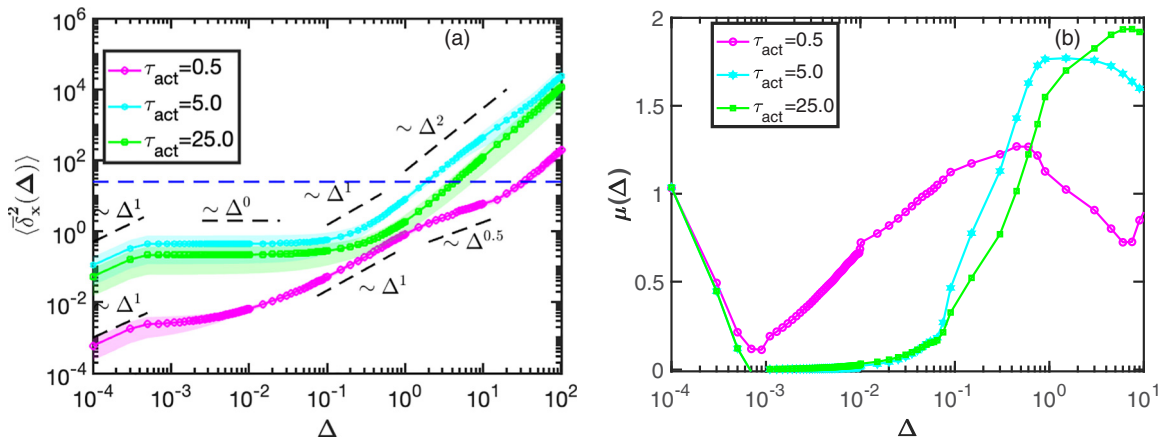


FIG. 13. The same as in Fig. 2, but plotted for a fixed $Pe = 1$ and for varying τ_{act} values (see the legend; $\sigma_t = 5$, $N = 15$, $T = 5 \times 10^2$). S-shaped variation of $\mu(\Delta)$ for large activity values is visible; see the text for details. The dashed blue line in panel (a) is the square of the cell size.

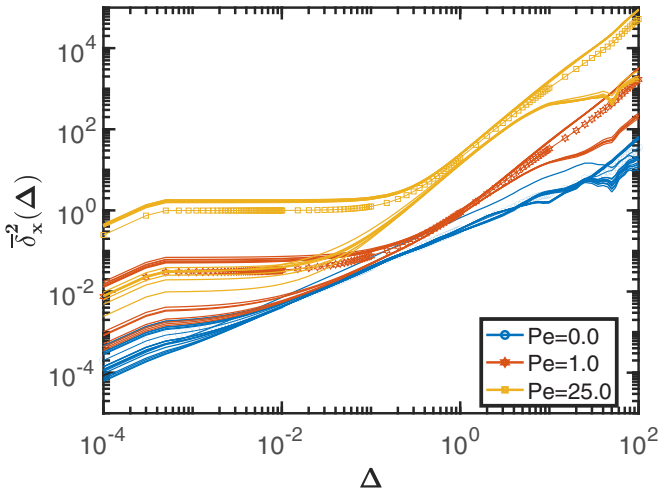


FIG. 14. Spread of individual TAMSDs used to generate the mean TAMSD (denoted here by the thick solid lines of respective colors) shown in Fig. 2(a) for the diffusion of AOUPs.

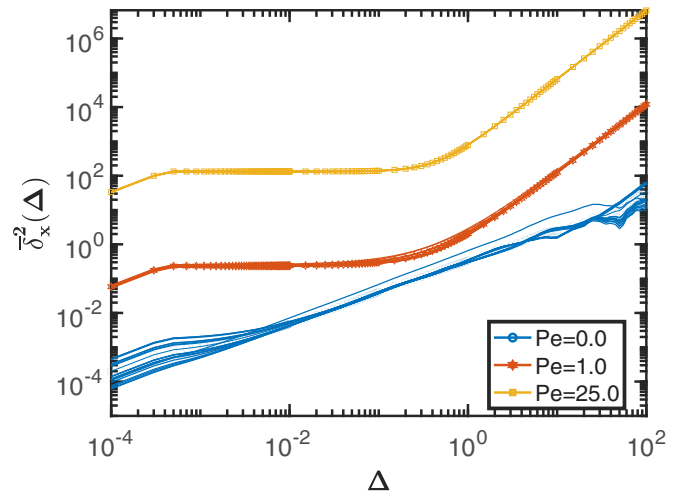


FIG. 15. The same as in Fig. 14, but for the dispersion of TAMSDs for the diffusion of RTPs shown in Fig. 3.

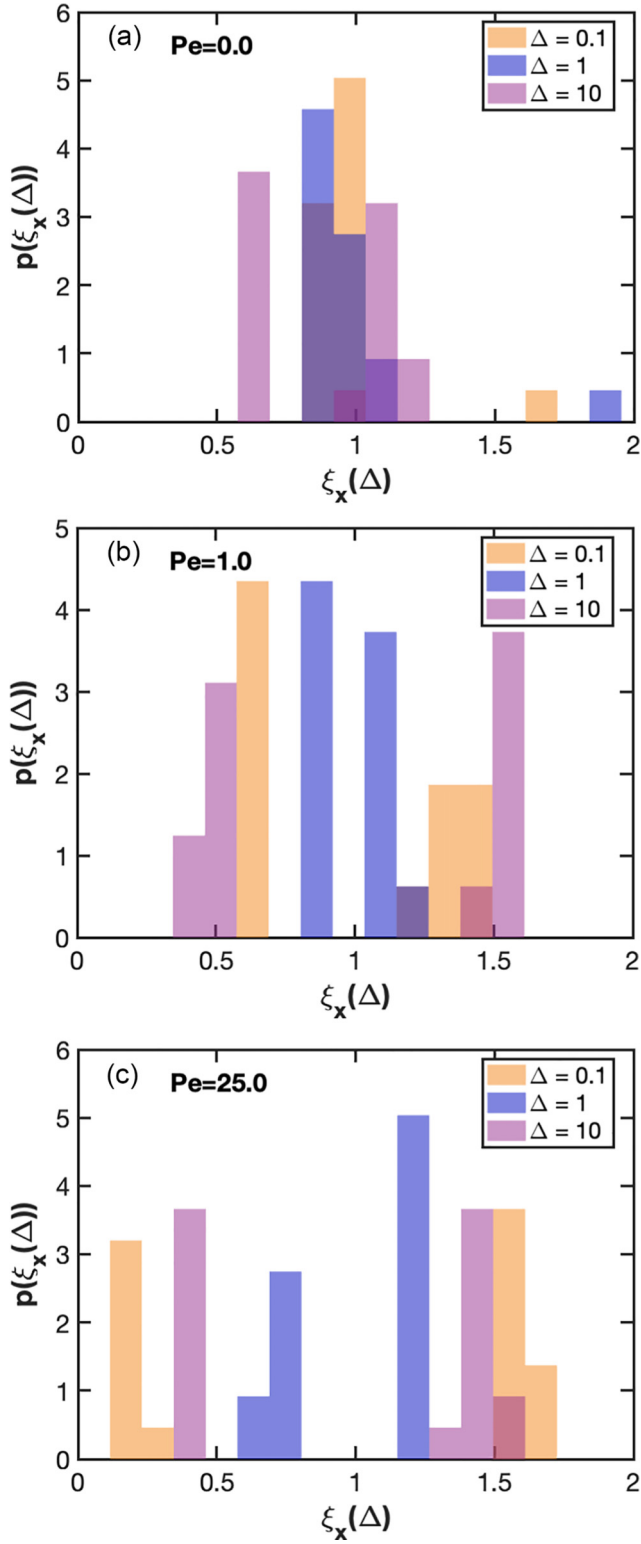


FIG. 16. Histograms representing the distributions of individual TAMSDs in 1D with $\xi_x(\Delta)$ given by (28) at three values of the lag time (see the legend) for varying activities (Péclet numbers) of AOUPs. These plots correspond to the TAMSDs presented in Fig. 14, computed at the same values of the model parameters.

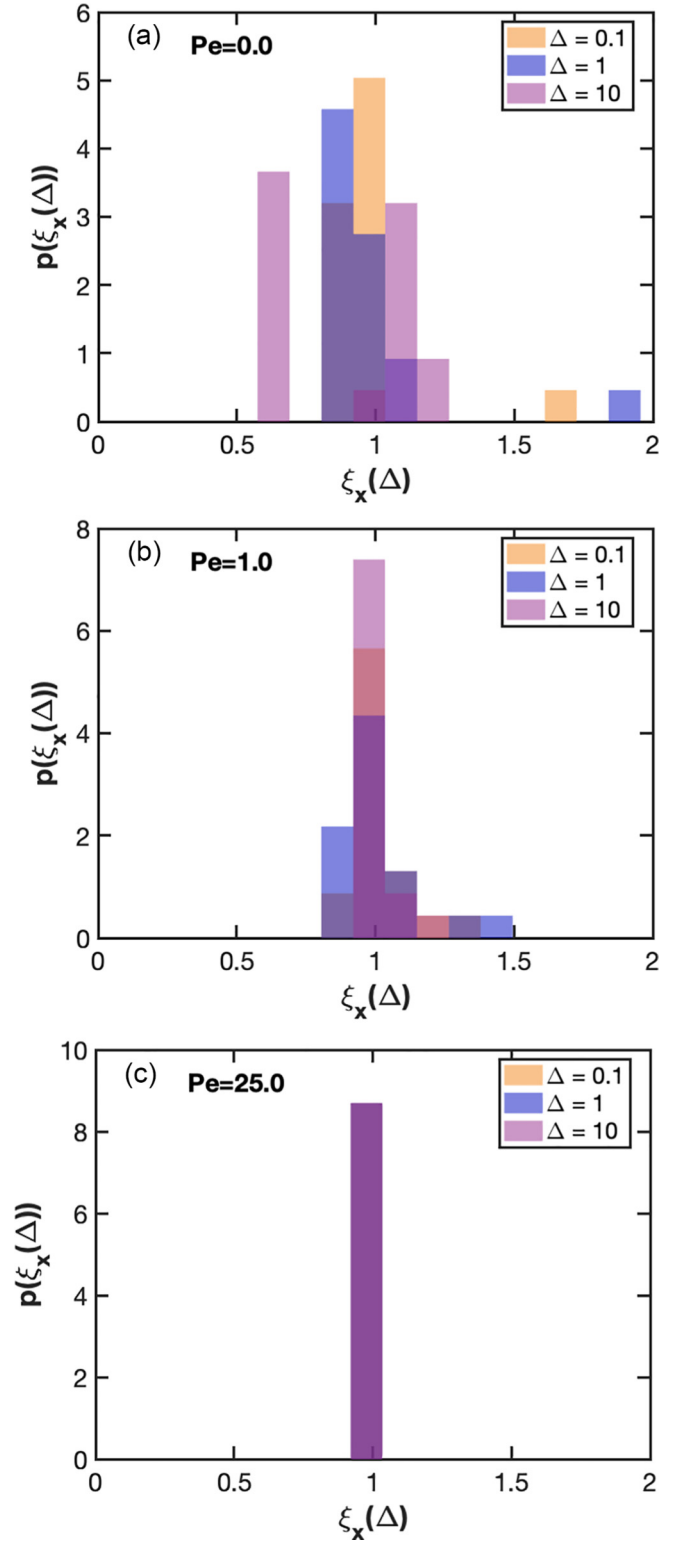


FIG. 17. The same as in Fig. 16, but for RTPs. This graph shows the same TAMSDs as in Fig. 15.

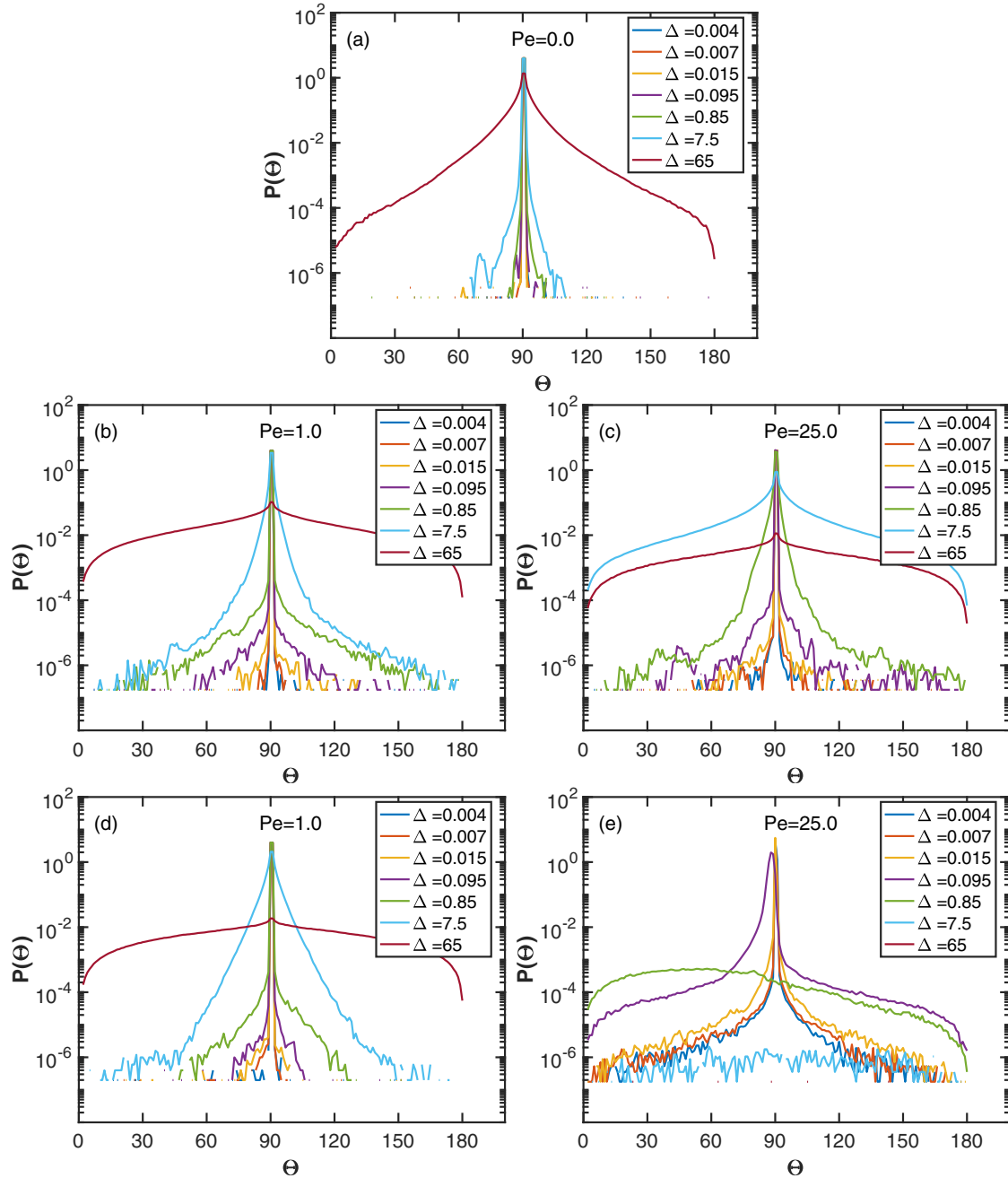


FIG. 18. Ensemble-and-time averaged PDFs $P(\Theta)$ given by Eq. (35) plotted as a function of the angle Θ defined by expression (34). The plots illustrate the results for passive tracers (a), AOUPs (b), (c), and for RTPs (d), (e) at various values of the lag time (see the legend). In panels (a)–(c) the parameters are the same as in Fig. 2, while in panels (d), (e) the parameters are as in Fig. 3.

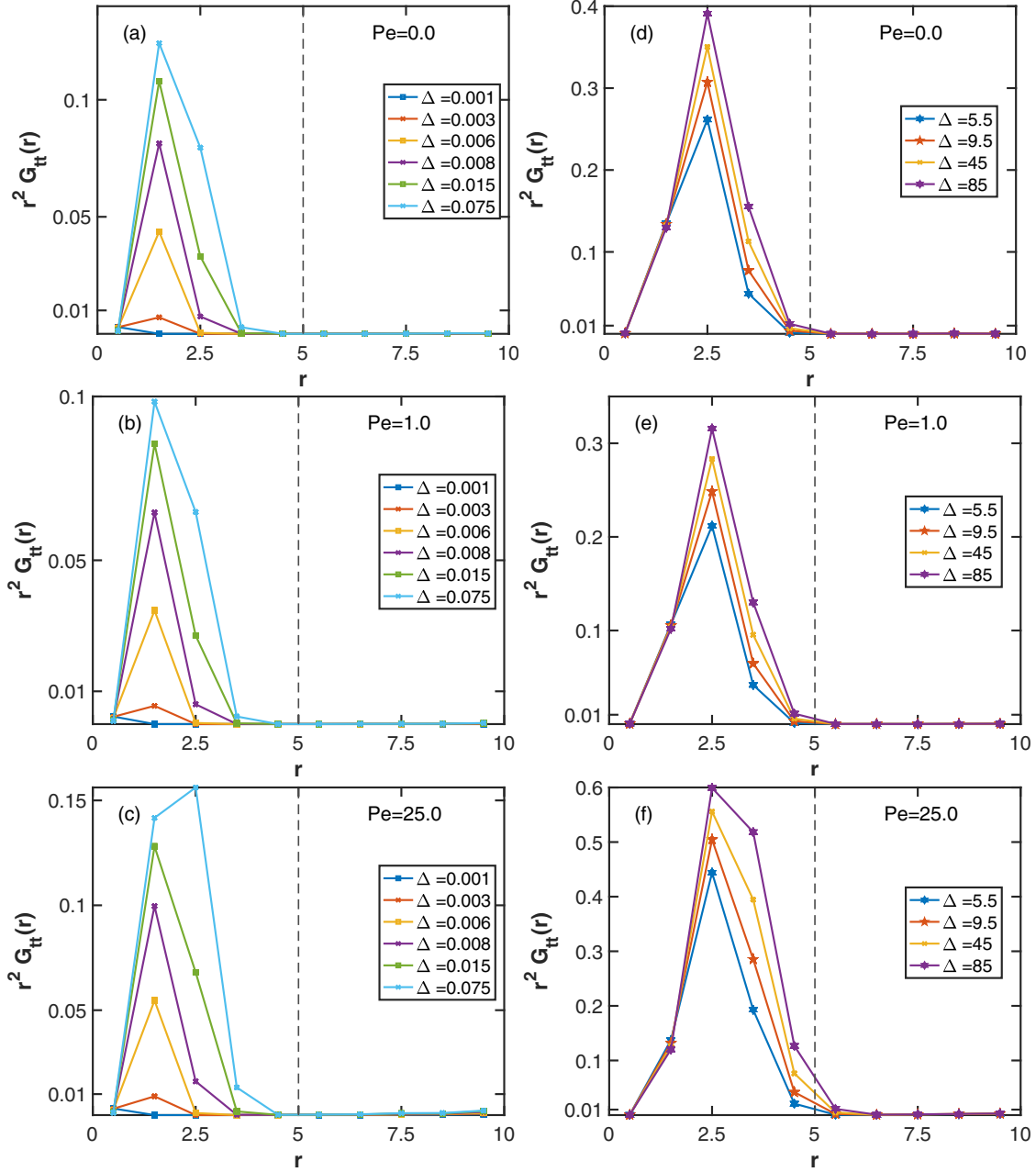


FIG. 19. Radial PDFs (32) of AOUPs for different activities of the tracers, shown as functions of the radial distance r (in units of σ_g) at short (a)–(c) and longer (d)–(f) lag times (see the legend for Δ values). The dashed vertical line corresponds to the mesh size of the network. Other parameters are the same as in Fig. 6.

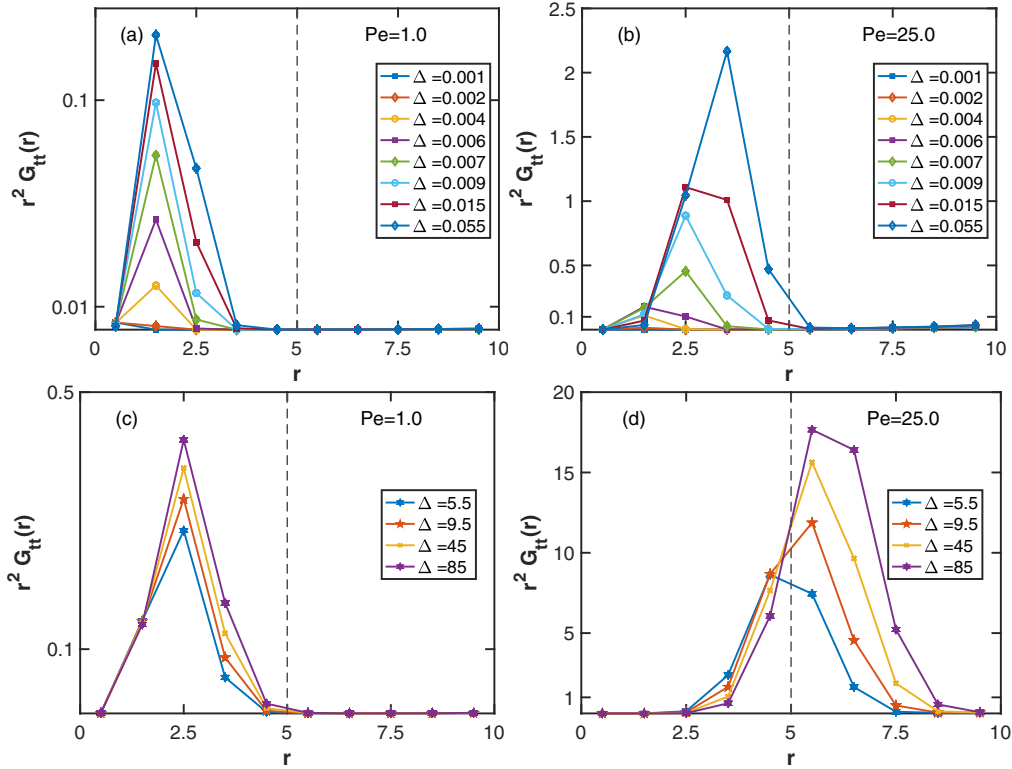


FIG. 20. The same as in Fig. 19, but instead computed for RTPs at different activity values at short (a), (b) and longer (c), (d) lag times. The panels (a) and (b) from Fig. 19 for passive particles complete these plots for the case $Pe = 0$. The parameters are as in Fig. 7.

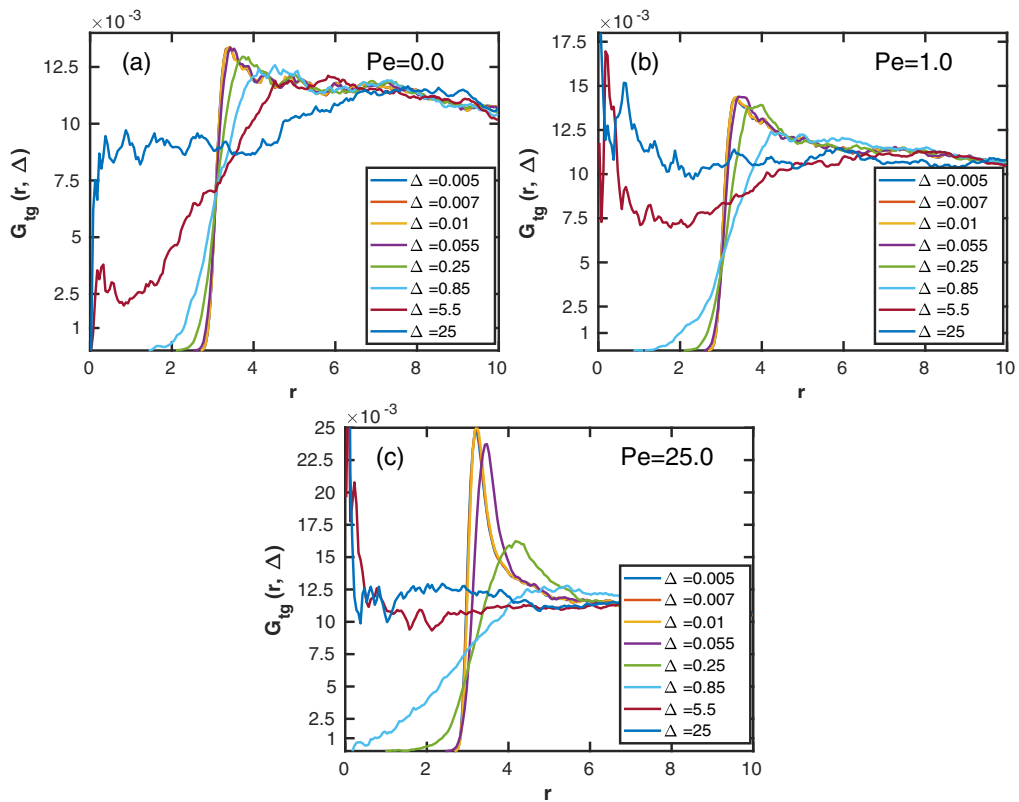


FIG. 21. Cross-HCF functions (33) plotted vs the distance r (in units of σ_g) for various lag times (as indicated in the legend) for three Pe values for the case of AOPs. Other parameters are the same as in Fig. 2.

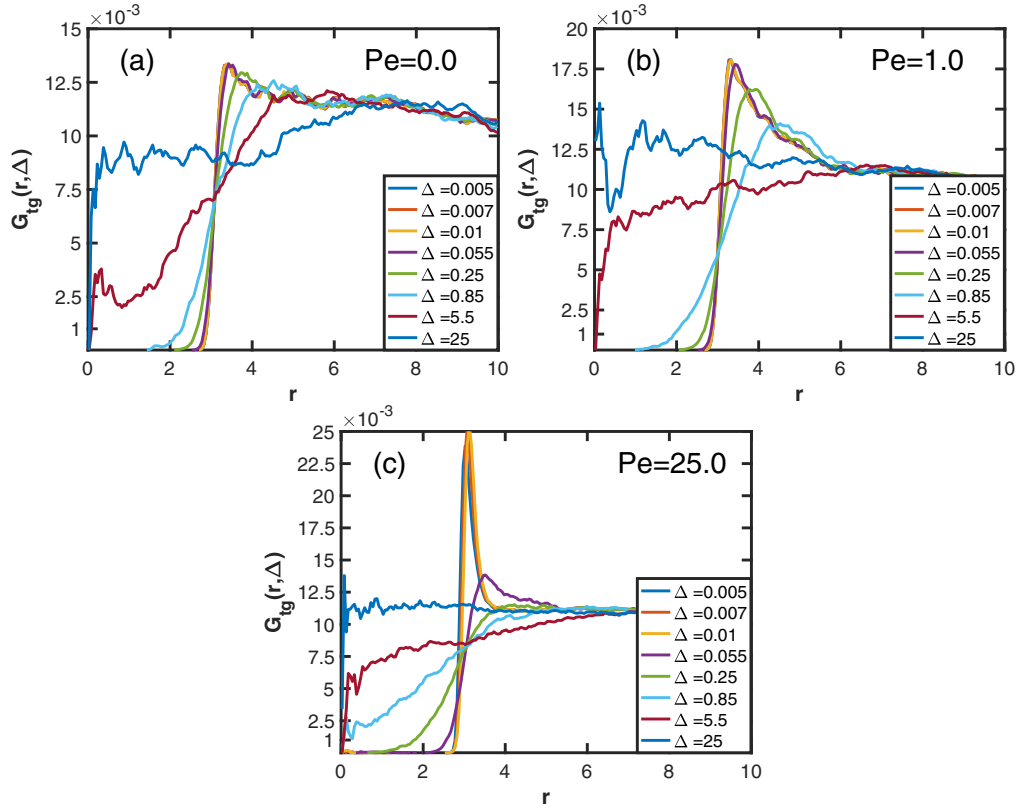


FIG. 22. The same as in Fig. 21, but for the case of RTPs at $Pe = 0.0$ (a), $Pe = 1.0$ (b), and $Pe = 25.0$ (c). Other parameters are the same as in Fig. 3.

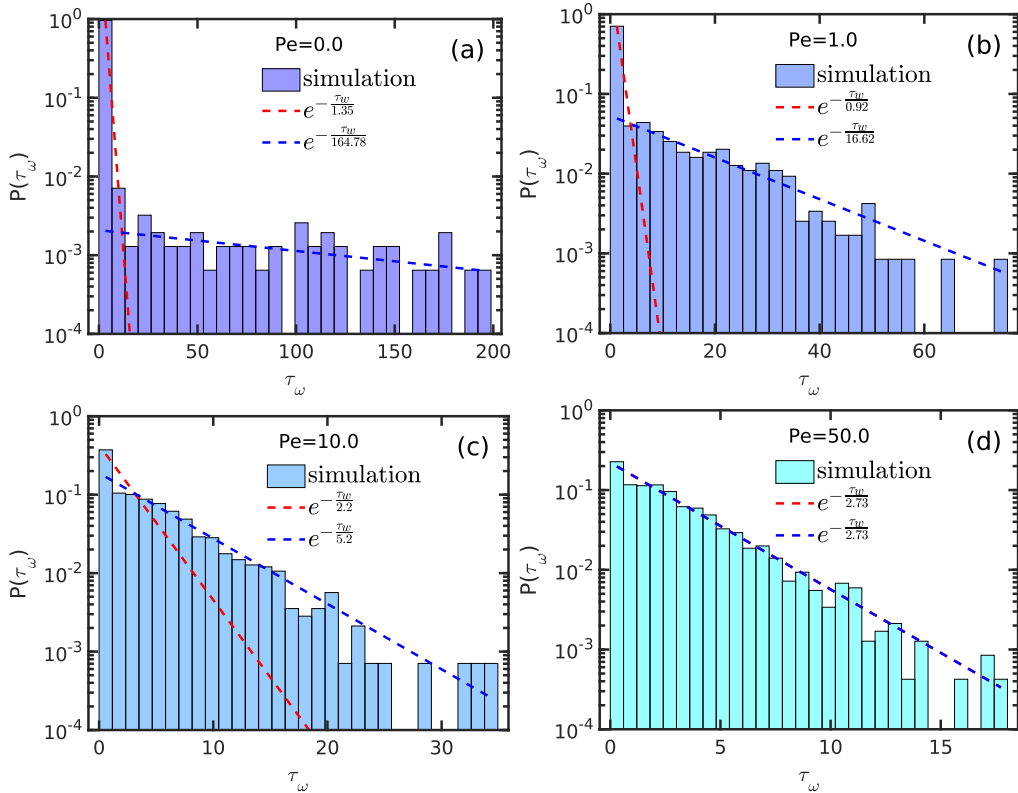


FIG. 23. Histograms of the PDFs of the WTDs for varying values of the Péclet number for the case of AOUPs. The dashed red and dashed blue lines are the two exponential fit functions, shown for the purpose of data comparison. At $Pe = 50$ in panel (d) a single exponential function provides a good fit to the simulation results. Other parameters are the same as in Fig. 2.

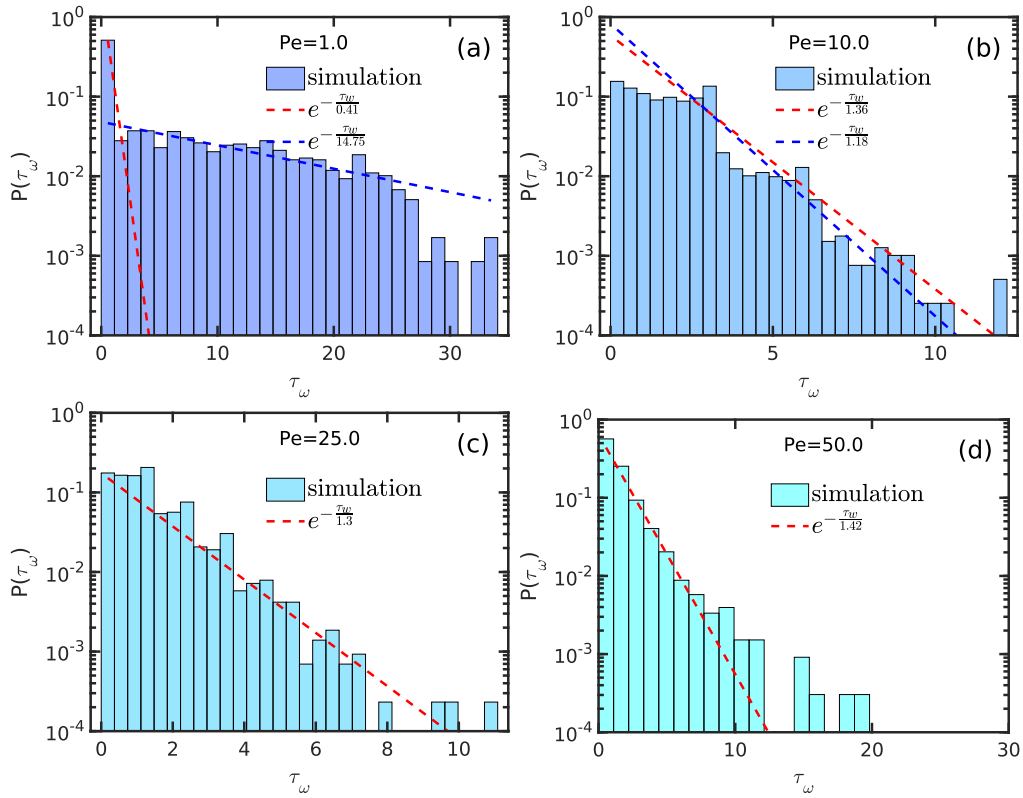


FIG. 24. The same as in Fig. 23, but for RTPs. The obtained PDFs of the WTDs cannot be fitted satisfactorily by a single- or by a double-exponential function. Other parameters are the same as in Fig. 3.

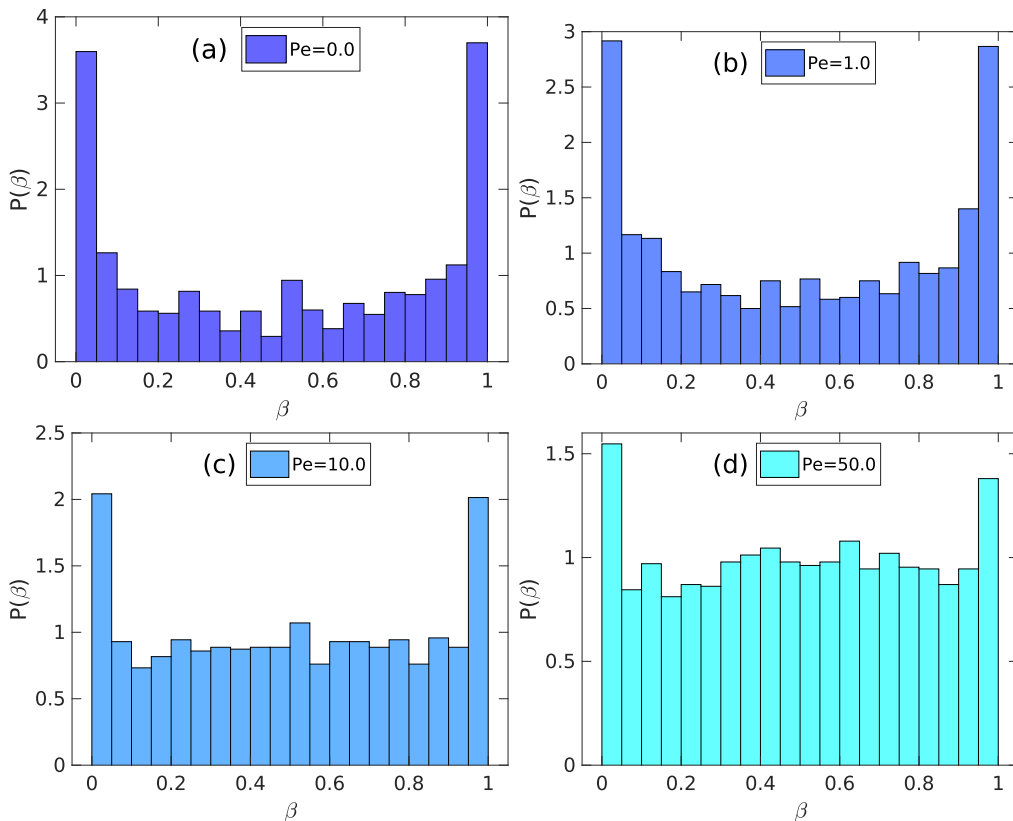


FIG. 25. PDFs of the UI (41) for the case of AOUPs corresponding to the situations and model parameters of Fig. 23.

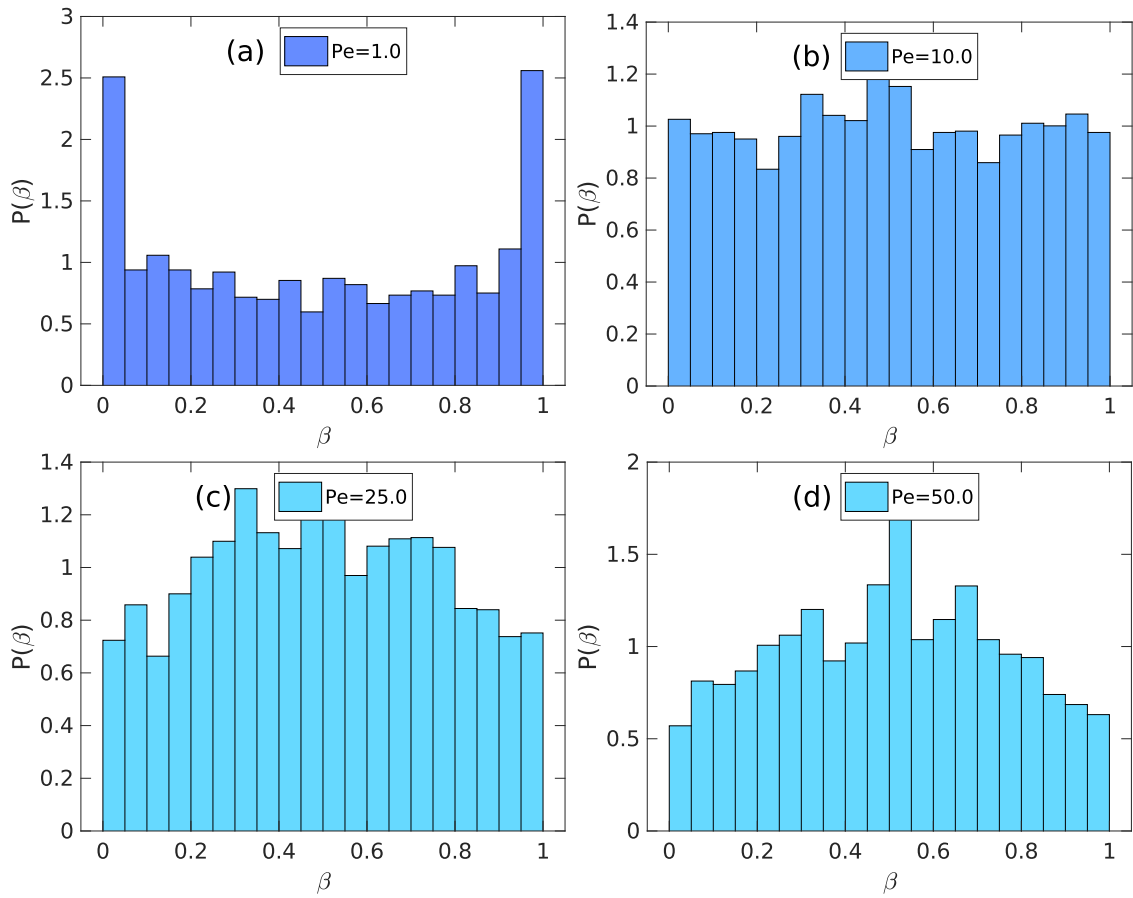


FIG. 26. The same as in Fig. 25, but for the case of RTPs, examined for the situations and model parameters of Fig. 24.

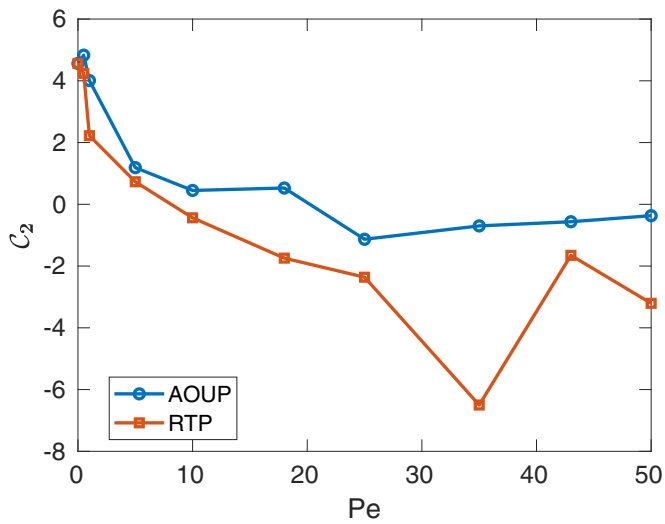


FIG. 27. C_2 coefficient in Eq. (47) plotted vs the Péclet number for the cases of diffusion of AOUPs and of RTPs.

- [1] R. Fürth, Die Brownsche Bewegung bei Berücksichtigung einer Persistenz der Bewegungsrichtung. Mit Anwendungen auf die Bewegung lebender Infusorien, *Z. Phys.* **2**, 244 (1920).
- [2] T. Vicsek, A. Czirók, E. Ben-Jacob, I. Cohen, and O. Shochet, Novel type of phase transition in a system of self-driven particles, *Phys. Rev. Lett.* **75**, 1226 (1995).
- [3] S. Ramaswamy, The mechanics and statistics of active matter, *Annu. Rev. Condens. Matter Phys.* **1**, 323 (2010).
- [4] P. Romanczuk, M. Bär, W. Ebeling, B. Lindner, and L. Schimansky-Geier, Active Brownian particles, *Eur. Phys. J.: Spec. Top.* **202**, 1 (2012).
- [5] C. Bechinger, R. Di Leonardo, H. Löwen, C. Reichhardt, G. Volpe, and G. Volpe, Active particles in complex and crowded environments, *Rev. Mod. Phys.* **88**, 045006 (2016).
- [6] J. Elgeti, R. G. Winkler, and G. Gompper, Physics of microswimmers—Single particle motion and collective behavior: a review, *Rep. Prog. Phys.* **78**, 056601 (2015).
- [7] A. G. Cherstvy, O. Nagel, C. Beta, and R. Metzler, Non-Gaussianity, population heterogeneity, and transient superdiffusion in the spreading dynamics of amoeboid cells, *Phys. Chem. Chem. Phys.* **20**, 23034 (2018).
- [8] M. Bär, R. Großmann, S. Heidenreich, and F. Peruani, Self-propelled rods: insights and perspectives for active matter, *Annu. Rev. Condens. Matter Phys.* **11**, 441 (2020).
- [9] G. Gompper, R. G. Winkler, T. Speck, A. Solon, C. Nardini, F. Peruani, H. Löwen, R. Golestanian, U. B. Kaupp, L. Alvarez, T. Kiorboe, E. Lauga, W. C. K. Poon, A. DeSimone, S. Muinos-Landin, A. Fischer, N. A. Söker, F. Cichos, R. Kapral, P. Gaspard *et al.*, The 2020 motile active matter roadmap, *J. Phys.: Condens. Matter* **32**, 193001 (2020).
- [10] H. Chate, Dry aligning dilute active matter, *Annu. Rev. Condens. Matter Phys.* **11**, 189 (2020).
- [11] L. Balasubramaniam, A. Doostmohammadi, T. B. Saw, G. H. N. S. Narayana, R. Mueller, T. Dang, M. Thomas, S. Gupta, S. Sonam, A. S. Yap *et al.*, Investigating the nature of active forces in tissues reveals how contractile cells can form extensile monolayers, *Nat. Mater.* **20**, 1156 (2021).
- [12] A. Ziepkke, I. Maryshev, I. S. Aranson, and E. Frey, Multi-scale organization in communicating active matter, *Nat. Commun.* **13**, 6727 (2022).
- [13] R. Adkins, I. Kolvin, Z. You, S. Witthaus, C. Marchetti, and Z. Dogic, Dynamics of active liquid interfaces, *Science* **377**, 768 (2022).
- [14] S. Shankar, A. Souslov, M. J. Bowick, C. Marchetti, and V. Vitelli, Topological active matter, *Nat. Rev. Phys.* **4**, 380 (2022).
- [15] M. Nasiri, E. Loran, and B. Liebchen, Smart active particles learn and transcend bacterial foraging strategies, *Proc. Natl. Acad. Sci. USA* **121**, e2317618121 (2024).
- [16] X. Fang, K. Kruse, T. Lu, and J. Wang, Nonequilibrium physics in biology, *Rev. Mod. Phys.* **91**, 045004 (2019).
- [17] R. Shaebani, A. Wysocki, R. G. Winkler, G. Gompper, and H. Rieger, Computational models for active matter, *Nat. Rev. Phys.* **2**, 181 (2020).
- [18] K. Drescher, R. E. Goldstein, N. Michel, M. Polin, and I. Tuval, Direct measurement of the flow field around swimming microorganisms, *Phys. Rev. Lett.* **105**, 168101 (2010).
- [19] R. Zenit and J. J. Feng, Hydrodynamic interactions among bubbles, drops, and particles in non-Newtonian liquids, *Annu. Rev. Fluid Mech.* **50**, 505 (2018).
- [20] R. Brown, A brief account of microscopical observations made in the months of June, July and August 1827, on the particles contained in the pollen of plants; and on the general existence of active molecules in organic and inorganic bodies, *Philos. Mag.* **4**, 161 (1828).
- [21] S. Burov, J.-H. Jeon, R. Metzler, and E. Barkai, Single particle tracking in systems showing anomalous diffusion: the role of weak ergodicity breaking, *Phys. Chem. Chem. Phys.* **13**, 1800 (2011).
- [22] R. Metzler, J.-H. Jeon, A. G. Cherstvy, and E. Barkai, Anomalous diffusion models and their properties: non-stationarity, non-ergodicity, and ageing at the centenary of single particle tracking, *Phys. Chem. Chem. Phys.* **16**, 24128 (2014).
- [23] N. C. Darnton, L. Turner, S. Rojevsky, and H. C. Berg, On torque and tumbling in swimming *Escherichia coli*, *J. Bacteriol.* **189**, 1756 (2007).
- [24] N. C. Darnton, L. Turner, S. Rojevsky, and H. C. Berg, Dynamics of bacterial swarming, *Biophys. J.* **98**, 2082 (2010).
- [25] A. Baskaran and C. Marchetti, Statistical mechanics and hydrodynamics of bacterial suspensions, *Proc. Natl. Acad. Sci. USA* **106**, 15567 (2009).
- [26] A. Jepson, V. A. Martinez, J. Schwarz-Linek, A. Morozov, and W. C. K. Poon, Enhanced diffusion of nonswimmers in a three-dimensional bath of motile bacteria, *Phys. Rev. E* **88**, 041002(R) (2013).
- [27] J. Gachelin, A. Rousselet, A. Lindner, and E. Clement, Collective motion in an active suspension of *Escherichia coli* bacteria, *New J. Phys.* **16**, 025003 (2014).
- [28] G. Ariel, A. Rabani, S. Benisty, J. D. Partridge, R. M. Harshey, and A. Be'er, Swarming bacteria migrate by Lévy walk, *Nat. Commun.* **6**, 8396 (2015).
- [29] N. Wadhwa and H. C. Berg, Bacterial motility: machinery and mechanisms, *Nat. Rev. Microbiol.* **20**, 161 (2022).
- [30] B. Ilkanaiv, D. B. Kearns, G. Ariel, and A. Be'er, Effect of cell aspect ratio on swarming bacteria, *Phys. Rev. Lett.* **118**, 158002 (2017).
- [31] J. M. Keestra, F. Carrara, and R. Stocker, The ecological roles of bacterial chemotaxis, *Nat. Rev. Microbiol.* **20**, 491 (2022).
- [32] K. M. Thormann, C. Beta, and M. J. Kühn, Wrapped up: the motility of polarly flagellated bacteria, *Annu. Rev. Microbiol.* **76**, 349 (2022).
- [33] R. S. Negi, R. G. Winkler, and G. Gompper, Collective behavior of self-steering active particles with velocity alignment and visual perception, *Phys. Rev. Res.* **6**, 013118 (2024).
- [34] T. Sanchez, D. T. N. Chen, S. J. DeCamp, M. Heymann, and Z. Dogic, Spontaneous motion in hierarchically assembled active matter, *Nature (London)* **491**, 431 (2012).
- [35] J. Prost, F. Jülicher, and J.-F. Joanny, Active gel physics, *Nat. Phys.* **11**, 111 (2015).
- [36] H. V. Goodson and E. M. Jonasson, Microtubules and microtubule-associated proteins, *Cold Spring Harbor Perspect. Biol.* **10**, a022608 (2018).
- [37] B. Gouveia, Y. Kim, J. W. Shaevitz, S. Petry, H. A. Stone, and C. P. Brangwynne, Capillary forces generated by biomolecular condensates, *Nature (London)* **609**, 255 (2022).
- [38] C. S. Korosec, I. N. Unksöv, P. Surendiran, R. Lyttleton, P. M. G. Curmi, C. N. Angstmann, R. Eichhorn, H. Linke, and N. R. Forde, Motility of an autonomous protein-based artificial motor that operates via a burnt-bridge principle, *Nat. Commun.* **15**, 1511 (2024).

- [39] E. Lauga and T. R. Powers, The hydrodynamics of swimming microorganisms, *Rep. Prog. Phys.* **72**, 096601 (2009).
- [40] S. van Helvert, C. Storm, and P. Friedl, Mechanoreciprocity in cell migration, *Nat. Cell Biol.* **20**, 8 (2018).
- [41] K. C. Leptos, J. S. Guasto, J. P. Gollub, A. I. Pesci, and R. E. Goldstein, Dynamics of enhanced tracer diffusion in suspensions of swimming eukaryotic microorganisms, *Phys. Rev. Lett.* **103**, 198103 (2009).
- [42] M. Knežević, T. Welker, and H. Stark, Collective motion of active particles exhibiting non-reciprocal orientational interactions, *Sci. Rep.* **12**, 19437 (2022).
- [43] R. Großmann, L. S. Bort, T. Moldenhawer, M. Stange, S. S. Panah, R. Metzler, and C. Beta, Non-Gaussian displacements in active transport on a carpet of motile cells, *Phys. Rev. Lett.* **132**, 088301 (2024).
- [44] I. M. De la Fuente, J. Carrasco-Pujante, B. Camino-Pontes, M. Fedetz, C. Bringas, A. Perez-Samartín, G. Perez-Yarza, J. I. Lopez, I. Malaina, and J. M. Cortes, Systemic cellular migration: the forces driving the directed locomotion movement of cells, *PNAS Nexus* **3**, 171 (2024).
- [45] L. Tröger, F. Goirand, and K. Alim, Size-dependent self-avoidance enables superdiffusive migration in macroscopic unicellulars, *Proc. Natl. Acad. Sci. USA* **121**, e2312611121 (2024).
- [46] L. G. A. Alves, D. B. Scariot, R. R. Guimarães, C. V. Nakamura, R. S. Mendes, and H. V. Ribeiro, Transient superdiffusion and long-range correlations in the motility patterns of trypanosomatid flagellate protozoa, *PLoS ONE* **11**, e0152092 (2016).
- [47] J. Saragosti, V. Calvez, N. Bournaveas, B. Perthame, A. Buguin, and P. Silberzan, Directional persistence of chemotactic bacteria in a traveling concentration wave, *Proc. Natl. Acad. Sci. USA* **108**, 16235 (2011).
- [48] S. Kamdar, S. Shin, P. Leishangthem, L. F. Francis, X. Xu, and X. Cheng, The colloidal nature of complex fluids enhances bacterial motility, *Nature (London)* **603**, 819 (2022).
- [49] A. Upadhyaya, J.-P. Rieu, J. A. Glazier, and Y. Sawada, Anomalous diffusion and non-Gaussian velocity distribution of Hydra cells in cellular aggregates, *Physica A* **293**, 549 (2001).
- [50] M. Polin, I. Tuval, K. Drescher, J. P. Gollub, and R. E. Goldstein, *Chlamydomonas* swims with two gears in a eukaryotic version of run-and-tumble locomotion, *Science* **325**, 487 (2009).
- [51] C. Jiang, H.-Y. Luo, X. Xu, S.-X. Dou, W. Li, D. Guan, F. Ye, X. Chen, M. Guo, P.-Y. Wang, and H. Li, Switch of cell migration modes orchestrated by changes of three-dimensional lamellipodium structure and intracellular diffusion, *Nat. Commun.* **14**, 5166 (2023).
- [52] T.-W. Su, I. Choi, J. Feng, K. Huang, E. McLeod, and A. Ozcan, Sperm trajectories form chiral ribbons, *Sci. Rep.* **3**, 1664 (2013).
- [53] J. F. Jikeli, L. Alvarez, B. M. Friedrich, L. G. Wilson, R. Pascal, R. Colin, M. Pichlo, A. Rennhack, C. Brenker, and U. B. Kaupp, Sperm navigation along helical paths in 3D chemoattractant landscapes, *Nat. Commun.* **6**, 7985 (2015).
- [54] O. Vilk, E. Aghion, T. Avgar, C. Beta, O. Nagel, A. Sabri, R. Sarfati, D. K. Schwartz, M. Weiss, D. Krapf, R. Nathan, R. Metzler, and M. Assaf, Unravelling the origins of anomalous diffusion: from molecules to migrating storks, *Phys. Rev. Res.* **4**, 033055 (2022).
- [55] D. S. Calovi, U. Lopez, S. Ngo, C. Sire, H. Chate, and G. Theraulaz, Swarming, schooling, milling: phase diagram of a data-driven fish school model, *New J. Phys.* **16**, 015026 (2014).
- [56] R. Nathan, C. T. Monk, R. Arlinghaus, T. Adam, J. Alos, M. Assaf, H. Baktoft, C. E. Beardsworth, M. G. Bertram, A. I. Bijleveld, T. Brodin, J. L. Brooks, A. Campos-Candela, S. J. Cooke, K. O. Gjelland, P. R. Gupte, R. Harel, G. Hellström, F. Jeltsch, S. S. Killen *et al.*, Big-data approaches lead to an increased understanding of the ecology of animal movement, *Science* **375**, eabg1780 (2022).
- [57] M. Roeleke, U. E. Schlägel, C. Gallagher, J. Pufelski, T. Blohm, R. Nathan, S. Toledo, F. Jeltsch, and C. C. Voigt, Insectivorous bats form mobile sensory networks to optimize prey localization: the case of the common noctule bat, *Proc. Natl. Acad. Sci. USA* **119**, e2203663119 (2022).
- [58] P. G. Meyer, A. G. Cherstvy, H. Seckler, R. Hering, N. Blaum, F. Jeltsch, and R. Metzler, Directedness, correlations, and daily cycles in springbok motion: from data via stochastic models to movement prediction, *Phys. Rev. Res.* **5**, 043129 (2023).
- [59] Z. Wu, Y. Chen, D. Mukasa, O. S. Pak, and W. Gao, Medical micro/nanorobots in complex media, *Chem. Soc. Rev.* **49**, 8088 (2020).
- [60] J. Yu, B. Wang, X. Du, Q. Wang, and L. Zhang, Ultra-extensible ribbon-like magnetic microswarm, *Nat. Commun.* **9**, 3260 (2018).
- [61] P. L. Venugopalan, B. Esteban-Fernández de Ávila, M. Pal, A. Ghosh, and J. Wang, Fantastic voyage of nanomotors into the cell, *ACS Nano* **14**, 9423 (2020).
- [62] W. Gao and J. Wang, The environmental impact of micro/nanomachines: a review, *ACS Nano* **8**, 3170 (2014).
- [63] J. Li, B. Esteban-Fernández de Ávila, W. Gao, L. Zhang, and J. Wang, Micro/nanorobots for biomedicine: delivery, surgery, sensing, and detoxification, *Sci. Robot.* **2**, eaam6431 (2017).
- [64] T. Bhattacharjee and S. S. Datta, Bacterial hopping and trapping in porous media, *Nat. Commun.* **10**, 2075 (2019).
- [65] H. Wu, B. Greydanus, and D. K. Schwartz, Mechanisms of transport enhancement for self-propelled nanoswimmers in a porous matrix, *Proc. Natl. Acad. Sci. USA* **118**, e2101807118 (2021).
- [66] C. Kurzthaler, S. Mandal, T. Bhattacharjee, H. Löwen, S. S. Datta, and H. A. Stone, A geometric criterion for the optimal spreading of active polymers in porous media, *Nat. Commun.* **12**, 7088 (2021).
- [67] H. Wu and D. K. Schwartz, Nanoparticle tracking to probe transport in porous media, *Acc. Chem. Res.* **53**, 2130 (2020).
- [68] N. Narinder, M. F. Bos, C. Abaurrea-Velasco, J. de Graaf, and C. Bechinger, Understanding enhanced rotational dynamics of active probes in rod suspensions, *Soft Matter* **18**, 6246 (2022).
- [69] B. Das, S. Paul, S. K. Manikandan, and A. Banerjee, Enhanced directionality of active processes in a viscoelastic bath, *New J. Phys.* **25**, 093051 (2023).
- [70] M. Shafiei Aporvari, M. Utkur, E. U. Saritas, G. Volpe, and J. Stenhammar, Anisotropic dynamics of a self-assembled colloidal chain in an active bath, *Soft Matter* **16**, 5609 (2020).
- [71] B. R. Ferrer, J. R. Gomez-Solano, and A. V. Arzola, Fluid viscoelasticity triggers fast transitions of a Brownian particle

- in a double well optical potential, *Phys. Rev. Lett.* **126**, 108001 (2021).
- [72] N. A. Bustos, C. M. Saad-Roy, A. G. Cherstvy, and C. E. Wagner, Distributed medium viscosity yields quasi-exponential step-size probability distributions in heterogeneous media, *Soft Matter* **18**, 8572 (2022).
- [73] D. Li, Y. Liu, H. Luo, and G. Jing, Anisotropic diffusion of elongated particles in active coherent flows, *Micromachines* **15**, 199 (2024).
- [74] K. Klett, A. G. Cherstvy, J. Shin, I. M. Sokolov, and R. Metzler, Non-Gaussian, transiently anomalous, and ergodic self-diffusion of flexible dumbbells in crowded two-dimensional environments: coupled translational and rotational motions, *Phys. Rev. E* **104**, 064603 (2021).
- [75] G. Anchutkin, V. Holubec, and F. Cichos, Run-and-tumble motion of ellipsoidal swimmers, [arXiv:2402.04697](https://arxiv.org/abs/2402.04697).
- [76] F. Höfling and T. Franosch, Anomalous transport in the crowded world of biological cells, *Rep. Prog. Phys.* **76**, 046602 (2013).
- [77] B. Monterosso, W. Margolin, A. J. Boersma, G. Rivas, B. Poolman, and S. Zorrilla, Macromolecular crowding, phase separation, and homeostasis in the orchestration of bacterial cellular functions, *Chem. Rev.* **124**, 1899 (2024).
- [78] C. Alfano, Y. Fichou, K. Huber, M. Weiss, E. Spruijt, S. Ebbinghaus, G. De Luca, M. A. Morando, V. Vetri, P. A. Temussi, and A. Pastore, Molecular crowding: the history and development of a scientific paradigm, *Chem. Rev.* **124**, 3186 (2024).
- [79] S. K. Ghosh, A. G. Cherstvy, D. S. Grebenkov, and R. Metzler, Anomalous, non-Gaussian tracer diffusion in crowded two-dimensional environments, *New J. Phys.* **18**, 013027 (2016).
- [80] J.-H. Jeon, M. Javanainen, H. Martinez-Seara, R. Metzler, and I. Vattulainen, Protein crowding in lipid bilayers gives rise to non-Gaussian anomalous lateral diffusion of phospholipids and proteins, *Phys. Rev. X* **6**, 021006 (2016).
- [81] J. Shin, A. G. Cherstvy, W. K. Kim, and R. Metzler, Facilitation of polymer looping and giant polymer diffusivity in crowded solutions of active particles, *New J. Phys.* **17**, 113008 (2015).
- [82] J. Shin, A. G. Cherstvy, W. K. Kim, and V. Ziburdaev, Elasticity-based polymer sorting in active fluids: a Brownian dynamics study, *Phys. Chem. Chem. Phys.* **19**, 18338 (2017).
- [83] C. Lozano, J. R. Gomez-Solano, and C. Bechinger, Active particles sense micromechanical properties of glasses, *Nat. Mater.* **18**, 1118 (2019).
- [84] J. Reichert, L. F. Granz, and T. Voigtman, Transport coefficients in dense active Brownian particle systems: mode-coupling theory and simulation results, *Eur. Phys. J. E* **44**, 27 (2021).
- [85] Y.-E. Keta, R. L. Jack, and L. Berthier, Disordered collective motion in dense assemblies of persistent particles, *Phys. Rev. Lett.* **129**, 048002 (2022).
- [86] J.-P. Bouchaud and A. Georges, Anomalous diffusion in disordered media: statistical mechanisms, models and physical applications, *Phys. Rep.* **195**, 127 (1990).
- [87] R. Metzler and J. Klafter, The random walk's guide to anomalous diffusion: a fractional dynamics approach, *Phys. Rep.* **339**, 1 (2000).
- [88] R. Metzler and J. Klafter, The restaurant at the end of the random walk: recent developments in the description of anomalous transport by fractional dynamics, *J. Phys. A: Math. Theor.* **37**, R161 (2004).
- [89] I. M. Sokolov, Models of anomalous diffusion in crowded environments, *Soft Matter* **8**, 9043 (2012).
- [90] E. Barkai, Y. Garini, and R. Metzler, Strange kinetics of single molecules in living cells, *Phys. Today* **65**(8), 29 (2012).
- [91] L. R. Evangelista and E. K. Lenzi, *Fractional Diffusion Equations and Anomalous Diffusion* (Cambridge University Press, Cambridge, 2018).
- [92] C. Manzo and M. F. Garcia-Parajo, A review of progress in single particle tracking: from methods to biophysical insights, *Rep. Prog. Phys.* **78**, 124601 (2015).
- [93] F. Simon, L. E. Weiss, and S. van Teeffelen, A guide to single-particle tracking, *Nat. Rev. Methods Primers* **4**, 66 (2024).
- [94] W. Wang, R. Metzler, and A. G. Cherstvy, Anomalous diffusion, aging, and nonergodicity of scaled Brownian motion with fractional Gaussian noise: overview of related experimental observations and models, *Phys. Chem. Chem. Phys.* **24**, 18482 (2022).
- [95] Y. Du, H. Jiang, and Z. Hou, Study of active Brownian particle diffusion in polymer solutions, *Soft Matter* **15**, 2020 (2019).
- [96] C. Yuan, A. Chen, B. Zhang, and N. Zhao, Activity-crowding coupling effect on the diffusion dynamics of a self-propelled particle in polymer solutions, *Phys. Chem. Chem. Phys.* **21**, 24112 (2019).
- [97] R. S. Yadav, C. Das, and R. Chakrabarti, Dynamics of a spherical self-propelled tracer in a polymeric medium: interplay of self-propulsion, stickiness, and crowding, *Soft Matter* **19**, 689 (2023).
- [98] W. Wang, L. A. Castro, M. Hoyos, and T. E. Mallouk, Autonomous motion of metallic microrods propelled by ultrasound, *ACS Nano* **6**, 6122 (2012).
- [99] A. E. Patteson, A. Gopinath, P. K. Purohit, and P. E. Arratia, Particle diffusion in active fluids is non-monotonic in size, *Soft Matter* **12**, 2365 (2016).
- [100] J. Yu, D. Jin, K.-F. Chan, Q. Wang, K. Yuan, and L. Zhang, Active generation and magnetic actuation of microrobotic swarms in bio-fluids, *Nat. Commun.* **10**, 5631 (2019).
- [101] A. R. Sprenger, M. A. Fernandez-Rodriguez, L. Alvarez, L. Isa, R. Wittkowski, and H. Löwen, Active Brownian motion with orientation-dependent motility: theory and experiments, *Langmuir* **36**, 7066 (2020).
- [102] F. Schweitzer, W. Ebeling, and B. Tilch, Complex motion of Brownian particles with energy depots, *Phys. Rev. Lett.* **80**, 5044 (1998).
- [103] O. Bénichou, A. Bodrova, D. Chakraborty, P. Illien, A. Law, C. Mejía-Monasterio, G. Oshanin, and R. Voituriez, Geometry-induced superdiffusion in driven crowded systems, *Phys. Rev. Lett.* **111**, 260601 (2013).
- [104] T. Bertrand, Y. Zhao, O. Bénichou, J. Tailleur, and R. Voituriez, Optimized diffusion of run-and-tumble particles in crowded environments, *Phys. Rev. Lett.* **120**, 198103 (2018).
- [105] R. Hou, A. G. Cherstvy, R. Metzler, and T. Akimoto, Biased continuous-time random walks for ordinary and equilibrium cases: facilitation of diffusion, ergodicity breaking and ageing, *Phys. Chem. Chem. Phys.* **20**, 20827 (2018).
- [106] L. Caprini and H. Löwen, Flocking without alignment interactions in attractive active Brownian particles, *Phys. Rev. Lett.* **130**, 148202 (2023).

- [107] I. Santra, U. Basu, and S. Sabhapandit, Run-and-tumble particles in two dimensions: marginal position distributions, *Phys. Rev. E* **101**, 062120 (2020).
- [108] J. Zhang, R. Alert, J. Yan, N. S. Wingreen, and S. Granick, Active phase separation by turning towards regions of higher density, *Nat. Phys.* **17**, 961 (2021).
- [109] M. Caraglio and T. Franosch, Analytic solution of an active Brownian particle in a harmonic well, *Phys. Rev. Lett.* **129**, 158001 (2022).
- [110] O. Granek, Y. Kafri, and J. Tailleur, Anomalous transport of tracers in active baths, *Phys. Rev. Lett.* **129**, 038001 (2022).
- [111] E. Lemaître, I. M. Sokolov, R. Metzler, and A. V. Chechkin, Non-Gaussian displacement distributions in models of heterogeneous active particle dynamics, *New J. Phys.* **25**, 013010 (2023).
- [112] C. Di Bello, R. Majumdar, R. Marathe, R. Metzler, and E. Roldan, Brownian particle in a Poisson-shot-noise active bath: exact statistics, effective temperature, and inference, *Ann. Phys.* **536**, 2300427 (2024).
- [113] Y. Zhao, C. Kurzthaler, N. Zhou, J. Schwarz-Linek, C. Devailly, J. Arlt, J.-D. Huang, W. C. K. Poon, T. Franosch, V. A. Martinez, and J. Tailleur, Quantitative characterization of run-and-tumble statistics in bulk bacterial suspensions, *Phys. Rev. E* **109**, 014612 (2024).
- [114] K. Suleiman, Y. Li, M. Abouagwa, and Y. Xu, Confinement effect on diffusion dynamics in active viscoelastic environments, *Eur. Phys. J. B* **97**, 49 (2024).
- [115] E. Kalz, A. Sharma, and R. Metzler, Field theory of active chiral hard disks: a first-principles approach to steric interactions, *J. Phys. A: Math. Theor.* **57**, 265002 (2024).
- [116] F. J. Sevilla, G. Chacon-Acosta, and T. Sandev, Anomalous diffusion of self-propelled particles, *J. Phys. A: Math. Theor.* **57**, 335004 (2024).
- [117] A. Datta, C. Beta, and R. Großmann, The random walk of intermittently self-propelled particles, [arXiv:2406.15277](https://arxiv.org/abs/2406.15277).
- [118] A. Datta, S. Beier, V. Pfeifer, R. Großmann, and C. Beta, Intermittent run motility of bacteria in gels exhibits power-law distributed dwell times, [arXiv:2408.02317](https://arxiv.org/abs/2408.02317).
- [119] B. Xue, Y. Liu, Y. Tian, and P. Yin, The coupling of rotational and translational dynamics for rapid diffusion of nanorods in macromolecular networks, *Nat. Commun.* **15**, 6502 (2024).
- [120] D. Baral, A. C. Lu, A. R. Bishop, K. O. Rasmussen, and N. K. Voulgarakis, Stochastically drifted Brownian motion for self-propelled particles, *Chaos Solitons Fractals* **187**, 115378 (2024).
- [121] J. Hansing and R. R. Netz, Hydrodynamic effects on particle diffusion in polymeric hydrogels with steric and electrostatic particle-gel interactions, *Macromolecules* **51**, 7608 (2018).
- [122] R. Shaebani and H. Rieger, Transient anomalous diffusion in run-and-tumble dynamics, *Front. Phys.* **7**, 120 (2019).
- [123] J. Schwarz-Linek, C. Valeriani, A. Cacciuto, M. E. Cates, D. Marenduzzo, A. N. Morozov, and W. C. K. Poon, Phase separation and rotor self-assembly in active particle suspensions, *Proc. Natl. Acad. Sci. USA* **109**, 4052 (2012).
- [124] P. A. Monderkamp, F. J. Schwarzendahl, M. A. Klatt, and H. Löwen, Active particles using reinforcement learning to navigate in complex motility landscapes, *Mach. Learn.: Sci. Technol.* **3**, 045024 (2022).
- [125] J. Katuri, R. Poehnl, A. Sokolov, W. Uspal, and A. Snezhko, Arrested-motility states in populations of shape-anisotropic active Janus particles, *Sci. Adv.* **8**, eabo3604 (2022).
- [126] C. Lohrmann and C. Holm, Optimal motility strategies for self-propelled agents to explore porous media, *Phys. Rev. E* **108**, 054401 (2023).
- [127] X.-B. Zhao, X. Zhang, and W. Guo, Diffusion of active Brownian particles under quenched disorder, *PLoS ONE* **19**, e0298466 (2024).
- [128] Y. Kim, W. K. Kim, and J.-H. Jeon, Active diffusion of self-propelled particles in semiflexible polymer networks, *Macromolecules* **57**, 7735 (2024).
- [129] M. Caraglio, H. Kaur, L. J. Fiderer, A. Lopez-Incera, H. J. Briegel, T. Franosch, and G. Munoz-Gil, Learning how to find targets in the micro-world: the case of intermittent active Brownian particles, *Soft Matter* **20**, 2008 (2024).
- [130] L. Theeyancheri, S. Chaki, T. Bhattacharjee, and R. Chakrabarti, Dynamic clustering of active rings, *Phys. Rev. Res.* **6**, L012038 (2024).
- [131] Y.-E. Keta, J. U. Klamsner, R. L. Jack, and L. Berthier, Emerging mesoscale flows and chaotic advection in dense active matter, *Phys. Rev. Lett.* **132**, 218301 (2024).
- [132] K. Suleiman, Y. Li, and Y. Xu, Non-Brownian dynamics of biased viscoelastic diffusion in Gaussian random environments, *Eur. Phys. J. Plus* **139**, 495 (2024).
- [133] R. Wiese, K. Kroy, and V. Holubec, Active Ornstein-Uhlenbeck model for bacterial heat engines, [arXiv:2406.19794](https://arxiv.org/abs/2406.19794).
- [134] É. Fodor, C. Nardini, M. E. Cates, J. Tailleur, P. Visco, and F. Van Wijland, How far from equilibrium is active matter? *Phys. Rev. Lett.* **117**, 038103 (2016).
- [135] K. Goswami and R. Metzler, Trapped tracer in a non-equilibrium bath: dynamics and energetics, *Soft Matter* **19**, 8802 (2023).
- [136] S. C. Takatori, R. De Dier, J. Vermant, and J. F. Brady, Acoustic trapping of active matter, *Nat. Commun.* **7**, 10694 (2016).
- [137] F. Schmidt, H. Šípová-Jungová, M. Käll, A. Würger, and G. Volpe, Non-equilibrium properties of an active nanoparticle in a harmonic potential, *Nat. Commun.* **12**, 1902 (2021).
- [138] I. S. Aranson and A. Pikovsky, Confinement and collective escape of active particles, *Phys. Rev. Lett.* **128**, 108001 (2022).
- [139] G. Du, F. Ye, and R. Podgornik, Trapping instability of an active particle in steering potential fields, *Phys. Rev. Res.* **4**, L042010 (2022).
- [140] R. Olfati-Saber, Flocking for multi-agent dynamic systems: algorithms and theory, *IEEE Trans. Autom. Control* **51**, 401 (2006).
- [141] H. Chaté, F. Ginelli, G. Grégoire, and F. Raynaud, Collective motion of self-propelled particles interacting without cohesion, *Phys. Rev. E* **77**, 046113 (2008).
- [142] M. R. D'Orsogna, Y.-L. Chuang, A. L. Bertozzi, and L. S. Chayes, Self-propelled particles with soft-core interactions: patterns, stability, and collapse, *Phys. Rev. Lett.* **96**, 104302 (2006).
- [143] E. S. Medeiros and U. Feudel, Local control for the collective dynamics of self-propelled particles, *Phys. Rev. E* **109**, 014312 (2024).
- [144] A. G. Cherstvy, DNA cholesteric phases: the role of DNA molecular chirality and DNA-DNA electrostatic interactions, *J. Phys. Chem. B* **112**, 12585 (2008).

- [145] A. G. Cherstvy, Electrostatic interactions in biological DNA-related systems, *Phys. Chem. Chem. Phys.* **13**, 9942 (2011).
- [146] A. Pikovsky, Transition to synchrony in chiral active particles, *J. Phys. Complex.* **2**, 025009 (2021).
- [147] A. Pattanayak, A. Shee, D. Chaudhuri, and A. Chaudhuri, Impact of torque on active Brownian particle: exact moments in two and three dimensions, *New J. Phys.* **26**, 083024 (2024).
- [148] K. Asheichyk, A. P. Solon, C. M. Rohwer, and M. Krüger, Response of active Brownian particles to shear flow, *J. Chem. Phys.* **150**, 144111 (2019).
- [149] A. Godec and R. Metzler, Active transport improves the precision of linear long distance molecular signalling, *J. Phys. A: Math. Theor.* **49**, 364001 (2016).
- [150] A. Godec and R. Metzler, Signal focusing through active transport, *Phys. Rev. E* **92**, 010701 (2015).
- [151] G. Bassu, M. Laurati, and E. Fratini, Transition from active motion to anomalous diffusion for *Bacillus subtilis* confined in hydrogel matrices, *Colloids Surf. B* **236**, 113797 (2024).
- [152] K. S. Olsen, L. Angheluta, and E. G. Flekkoy, Active Brownian particles moving through disordered landscapes, *Soft Matter* **17**, 2151 (2021).
- [153] A. G. Cherstvy, A. V. Chechkin, and R. Metzler, Particle invasion, survival, and non-ergodicity in 2D diffusion processes with space-dependent diffusivity, *Soft Matter* **10**, 1591 (2014).
- [154] H. Landfield, N. Kalamaris, and M. Wang, Extreme dependence of dynamics on concentration in highly crowded polyelectrolyte solutions, *Sci. Adv.* **10**, eado4976 (2024).
- [155] J. Shin, A. G. Cherstvy, and R. Metzler, Sensing viruses by mechanical tension of DNA in responsive hydrogels, *Phys. Rev. X* **4**, 021002 (2014).
- [156] V. Schaller, C. Weber, C. Semmrich, E. Frey, and A. R. Bausch, Polar patterns of driven filaments, *Nature (London)* **467**, 73 (2010).
- [157] A. G. Cherstvy, S. Thapa, C. E. Wagner, and R. Metzler, Non-Gaussian, non-ergodic, and non-Fickian diffusion of tracers in mucin hydrogels, *Soft Matter* **15**, 2526 (2019).
- [158] J. Li and D. J. Mooney, Designing hydrogels for controlled drug delivery, *Nat. Rev. Mater.* **1**, 16071 (2016).
- [159] Y. Ju, Y. Hu, P. Yang, X. Xie, and B. Fang, Extracellular vesicle-loaded hydrogels for tissue repair and regeneration, *Mater. Today Bio* **18**, 100522 (2023).
- [160] M. Kanduč, W. K. Kim, R. Roa, and J. Dzubiella, How the shape and chemistry of molecular penetrants control responsive hydrogel permeability, *ACS Nano* **15**, 614 (2021).
- [161] F. J. Vernerey, S. Lalitha Sridhar, A. Muralidharan, and S. J. Bryant, Mechanics of 3D cell-hydrogel interactions: experiments, models, and mechanisms, *Chem. Rev.* **121**, 11085 (2021).
- [162] M. L. Gardel, M. T. Valentine, J. C. Crocker, A. R. Bausch, and D. A. Weitz, Microrheology of entangled F-actin solutions, *Phys. Rev. Lett.* **91**, 158302 (2003).
- [163] M. Levin, G. Bel, and Y. Roichman, Measurements and characterization of the dynamics of tracer particles in an actin network, *J. Chem. Phys.* **154**, 144901 (2021).
- [164] C. E. Wagner, B. S. Turner, M. Rubinstein, G. H. McKinley, and K. Ribbeck, A rheological study of the association and dynamics of MUC5AC gels, *Biomacromolecules* **18**, 3654 (2017).
- [165] N. A. Bustos, K. Ribbeck, and C. E. Wagner, The role of mucosal barriers in disease progression and transmission, *Adv. Drug Delivery Rev.* **200**, 115008 (2023).
- [166] C. E. Wagner, K. M. Wheeler, and K. Ribbeck, Mucins and their role in shaping the functions of mucus barriers, *Annu. Rev. Cell Dev. Biol.* **34**, 189 (2018).
- [167] S. Thapa, M. A. Lomholt, J. Krog, A. G. Cherstvy, and R. Metzler, Bayesian analysis of single-particle tracking data using the nested-sampling algorithm: maximum-likelihood model selection applied to stochastic-diffusivity data, *Phys. Chem. Chem. Phys.* **20**, 29018 (2018).
- [168] S. K. Kumar, V. Ganesan, and R. A. Riggleman, Perspective: outstanding theoretical questions in polymer-nanoparticle hybrids, *J. Chem. Phys.* **147**, 020901 (2017).
- [169] H. Zhou and S. B. Chen, Brownian dynamics simulation of tracer diffusion in a cross-linked network, *Phys. Rev. E* **79**, 021801 (2009).
- [170] A. Godec, M. Bauer, and R. Metzler, Collective dynamics effect transient subdiffusion of inert tracers in flexible gel networks, *New J. Phys.* **16**, 092002 (2014).
- [171] N. Kamerlin and C. Elvingson, Tracer diffusion in a polymer gel: simulations of static and dynamic 3D networks using spherical boundary conditions, *J. Phys.: Condens. Matter* **28**, 475101 (2016).
- [172] M. Hu, H. Chen, H. Wang, S. Burov, E. Barkai, and D. Wang, Triggering Gaussian-to-exponential transition of displacement distribution in polymer nanocomposites via adsorption-induced trapping, *ACS Nano* **17**, 21708 (2023).
- [173] P. Kumar, L. Theeyancheri, S. Chaki, and R. Chakrabarti, Transport of probe particles in a polymer network: effects of probe size, network rigidity and probe-polymer interaction, *Soft Matter* **15**, 8992 (2019).
- [174] H. W. Cho, H. Kim, B. J. Sung, and J. S. Kim, Tracer diffusion in tightly-meshed homogeneous polymer networks: a Brownian dynamics simulation study, *Polymers* **12**, 2067 (2020).
- [175] V. Sorichetti, V. Hugouvieux, and W. Kob, Dynamics of nanoparticles in polydisperse polymer networks: from free diffusion to hopping, *Macromolecules* **54**, 8575 (2021).
- [176] A. Mansuri, P. Vora, T. Feuerbach, J. Winck, A. W. P. Vermeer, W. Hoheisel, J. Kierfeld, and M. Thommes, A Monte Carlo simulation of tracer diffusion in amorphous polymers, *Soft Matter* **20**, 6204 (2024).
- [177] Y. Kim, S. Joo, W. K. Kim, and J.-H. Jeon, Active diffusion of self-propelled particles in flexible polymer networks, *Macromolecules* **55**, 7136 (2022).
- [178] Y. Lu, X.-Y. Liu, and G.-H. Hu, Double-spring model for nanoparticle diffusion in a polymer network, *Macromolecules* **55**, 4548 (2022).
- [179] P. Kumar and R. Chakrabarti, Dynamics of self-propelled tracer particles inside a polymer network, *Phys. Chem. Chem. Phys.* **25**, 1937 (2023).
- [180] See Supplemental Material at <http://link.aps.org/supplemental/10.1103/PhysRevE.110.044609> for additional video files illustrating the dynamics.
- [181] A. G. Cherstvy, W. Wang, R. Metzler, and I. M. Sokolov, Inertia triggers nonergodicity of fractional Brownian motion, *Phys. Rev. E* **104**, 024115 (2021).
- [182] F. Mori, P. Le Doussal, S. N. Majumdar, and G. Schehr, Universal survival probability for a d-dimensional run-and-tumble particle, *Phys. Rev. Lett.* **124**, 090603 (2020).

- [183] G. E. Uhlenbeck and L. S. Ornstein, On the theory of the Brownian motion, *Phys. Rev.* **36**, 823 (1930).
- [184] K. Goswami and K. L. Sebastian, Diffusion caused by two noises—active and thermal, *J. Stat. Mech.: Theory Exp.* (2019) 083501.
- [185] D. Martin, J. O’Byrne, M. E. Cates, É. Fodor, C. Nardini, J. Tailleur, and F. Van Wijland, Statistical mechanics of active Ornstein-Uhlenbeck particles, *Phys. Rev. E* **103**, 032607 (2021).
- [186] L. Caprini, A. R. Sprenger, H. Löwen, and R. Wittmann, The parental active model: a unifying stochastic description of self-propulsion, *J. Chem. Phys.* **156**, 071102 (2022).
- [187] K. Goswami and R. Metzler, Effects of active noise on transition-path dynamics, *J. Phys. Complex.* **4**, 025005 (2023).
- [188] F. J. Sevilla, R. F. Rodríguez, and J. R. Gomez-Solano, Generalized Ornstein-Uhlenbeck model for active motion, *Phys. Rev. E* **100**, 032123 (2019).
- [189] K. Goswami, Inertial particle under active fluctuations: diffusion and work distributions, *Phys. Rev. E* **105**, 044123 (2022).
- [190] T. Demaerel and C. Maes, Active processes in one dimension, *Phys. Rev. E* **97**, 032604 (2018).
- [191] U. Basu, S. N. Majumdar, A. Rosso, S. Sabhapandit, and G. Schehr, Exact stationary state of a run-and-tumble particle with three internal states in a harmonic trap, *J. Phys. A: Math. Theor.* **53**, 09LT01 (2020).
- [192] D. Barik, P. K. Ghosh, and D. S. Ray, Langevin dynamics with dichotomous noise; direct simulation and applications, *J. Stat. Mech.: Theory Exp.* (2006) P03010.
- [193] P. Jung and P. Hänggi, Dynamical systems: a unified colored-noise approximation, *Phys. Rev. A* **35**, 4464 (1987).
- [194] P. M. Morse, Diatomic molecules according to the wave mechanics. II. Vibrational levels, *Phys. Rev.* **34**, 57 (1929).
- [195] J. E. Lennard-Jones, The electronic structure of some diatomic molecules, *Trans. Faraday Soc.* **25**, 668 (1929).
- [196] R. A. Buckingham and J. E. Lennard-Jones, The classical equation of state of gaseous helium, neon and argon, *Proc. Royal Soc. London Ser. A* **168**, 264 (1938).
- [197] G. Mie, Zur kinetischen Theorie der einatomigen Körper, *Ann. Phys.* **316**, 657 (1903).
- [198] H. C. Andersen, J. D. Weeks, and D. Chandler, Relationship between the hard-sphere fluid and fluids with realistic repulsive forces, *Phys. Rev. A* **4**, 1597 (1971).
- [199] J. D. Weeks, D. Chandler, and H. C. Andersen, Role of repulsive forces in determining the equilibrium structure of simple liquids, *J. Chem. Phys.* **54**, 5237 (1971).
- [200] M. P. Allen and D. J. Tildesley, *Computer Simulations of Liquids* (Oxford, Clarendon, 1987).
- [201] A. G. Cherstvy, D. Vinod, E. Aghion, A. V. Chechkin, and R. Metzler, Time averaging, ageing and delay analysis of financial time series, *New J. Phys.* **19**, 063045 (2017).
- [202] L. Boltzmann, Ueber die Eigenschaften monocyclischer und anderer damit verwandter Systeme, *J. Reine Angew. Math.* **1885**, 68 (1885).
- [203] A. G. Cherstvy, H. Safdari, and R. Metzler, Anomalous diffusion, nonergodicity, and ageing for exponentially and logarithmically time-dependent diffusivity: striking differences for massive versus massless particles, *J. Phys. D* **54**, 195401 (2021).
- [204] W. Deng and E. Barkai, Ergodic properties of fractional Brownian-Langevin motion, *Phys. Rev. E* **79**, 011112 (2009).
- [205] W. Wang, A. G. Cherstvy, A. V. Chechkin, S. Thapa, F. Seno, X. Liu, and R. Metzler, Fractional Brownian motion with random diffusivity: emerging residual nonergodicity below the correlation time, *J. Phys. A: Math. Theor.* **53**, 474001 (2020).
- [206] D. Vinod, A. G. Cherstvy, W. Wang, R. Metzler, and I. M. Sokolov, Nonergodicity of reset geometric Brownian motion, *Phys. Rev. E* **105**, L012106 (2022).
- [207] Y. Liang, W. Wang, R. Metzler, and A. G. Cherstvy, Anomalous diffusion, nonergodicity, non-Gaussianity, and aging of fractional Brownian motion with nonlinear clocks, *Phys. Rev. E* **108**, 034113 (2023).
- [208] Y. Liang, W. Wang, R. Metzler, and A. G. Cherstvy, Nonergodicity of confined superdiffusive fractional Brownian motion, *Phys. Rev. E* **108**, L052101 (2023).
- [209] Y. He, S. Burov, R. Metzler, and E. Barkai, Random time-scale invariant diffusion and transport coefficients, *Phys. Rev. Lett.* **101**, 058101 (2008).
- [210] S. Kullback and R. A. Leibler, On information and sufficiency, *Ann. Math. Stat.* **22**, 79 (1951).
- [211] L. Van Hove, Correlations in space and time and Born approximation scattering in systems of interacting particles, *Phys. Rev.* **95**, 249 (1954).
- [212] N. Nahali and A. Rosa, Nanoprobe diffusion in entangled polymer solutions: linear vs. unconcatenated ring chains, *J. Chem. Phys.* **148**, 194902 (2018).
- [213] T. G. Mattos, C. Mejía-Monasterio, R. Metzler, and G. Oshanin, First passages in bounded domains: when is the mean first passage time meaningful? *Phys. Rev. E* **86**, 031143 (2012).
- [214] J. Rudnick and G. Gaspari, The asphericity of random walks, *J. Phys. A: Math. Gen.* **19**, L191 (1986).
- [215] J. Rudnick and G. Gaspari, The shapes of random walks, *Science* **237**, 384 (1987).
- [216] X. Michalet, Mean square displacement analysis of single-particle trajectories with localization error: Brownian motion in an isotropic medium, *Phys. Rev. E* **82**, 041914 (2010).
- [217] X. Michalet and A. J. Berglund, Optimal diffusion coefficient estimation in single-particle tracking, *Phys. Rev. E* **85**, 061916 (2012).
- [218] N. Klongvessa, F. Ginot, C. Ybert, C. Cottin-Bizonne, and M. Leocmach, Active glass: ergodicity breaking dramatically affects response to self-propulsion, *Phys. Rev. Lett.* **123**, 248004 (2019).
- [219] J. Reichert and T. Voigtmann, Tracer dynamics in crowded active-particle suspensions, *Soft Matter* **17**, 10492 (2021).
- [220] A. Biswas, J. M. Cruz, P. Parmananda, and D. Das, First passage of an active particle in the presence of passive crowders, *Soft Matter* **16**, 6138 (2020).
- [221] T. Debnath, P. Chaudhury, T. Mukherjee, D. Mondal, and P. K. Ghosh, Escape kinetics of self-propelled particles from a circular cavity, *J. Chem. Phys.* **155**, 194102 (2021).
- [222] P. Kumar and R. Chakrabarti, Escape dynamics of a self-propelled nanorod from circular confinements with narrow openings, *Soft Matter* **19**, 6743 (2023).
- [223] C. Li, Q. Chen, and M. Ding, Escape dynamics of active ring polymers in a cylindrical nanochannel, *Soft Matter* **20**, 1719 (2024).
- [224] B. Corci, O. Hooiveld, A. M. Dolga, and C. Åberg, Extending the analogy between intracellular motion in mammalian cells and glassy dynamics, *Soft Matter* **19**, 2529 (2023).

- [225] A. Joseph, C. Contini, D. Cecchin, S. Nyberg, L. Ruiz-Perez, J. Gaitzsch, G. Fullstone, X. Tian, J. Azizi, J. Preston *et al.*, Chemotactic synthetic vesicles: design and applications in blood-brain barrier crossing, *Sci. Adv.* **3**, e1700362 (2017).
- [226] F. Soto, J. Wang, R. Ahmed, and U. Demirci, Medical micro/nanorobots in precision medicine, *Adv. Sci.* **7**, 2002203 (2020).
- [227] K. A. Rose, N. Gogotsi, J. H. Galarraga, J. A. Burdick, C. B. Murray, D. Lee, and R. J. Composto, Shape anisotropy enhances nanoparticle dynamics in nearly homogeneous hydrogels, *Macromolecules* **55**, 8514 (2022).
- [228] R. Liu, C. Luo, Z. Pang, J. Zhang, S. Ruan, M. Wu, L. Wang, T. Sun, N. Li, L. Han *et al.*, Advances of nanoparticles as drug delivery systems for disease diagnosis and treatment, *Chin. Chem. Lett.* **34**, 107518 (2023).
- [229] N. Fakhri, F. C. MacKintosh, B. Lounis, L. Cognet, and M. Pasquali, Brownian motion of stiff filaments in a crowded environment, *Science* **330**, 1804 (2010).